# A review of label-free photonics-based techniques for cancer detection in the digestive and urinary systems

# A review of label-free photonics-based techniques for cancer detection in the digestive and urinary systems

To cite this article before publication: Gustavo Castro-Olvera *et al* 2024 *J. Phys. Photonics* in press https://doi.org/10.1088/2515-7647/ad8613

**IOP** Publishing Journal Title
Journal **XX** (XXXX) XXXXXX https://doi.org/XXXX/XXXX

# A review of label-free photonics-based techniques for cancer detection in the digestive and urinary systems

**Castro-Olvera, G.[1*+], Baria, E.[2,3*], Stoliarov, D.[4*], Morselli, S.[5,6], Orlandini, B.[7], Vanoni, M.[8], Sayinc, H.[9], Koviarov, A.[4], Galiakhmetova, D.[4], Dickie, J.[10], Cicchi, R.[2,3], Serni, S.[5,6], Gacci, M.[5,6], Ribal, M.J.[11], Pavone, F.S.[2,3,12], Loza-Alvarez, P.[1], Rafailov, E.[4] , Gumenyuk, R.[13]**

[1] ICFO-Institut de Ciencies Fotoniques, The Barcelona Institute of Science and Technology, 08860 Castelldefels (Barcelona), Spain
[2] National Institute of Optics, National Research Council (CNR-INO), 50019 Sesto Fiorentino, Italy
[3] LENS – European Laboratory for Non-linear Spectroscopy, 50019 Sesto Fiorentino, Italy
[4] Aston Institute of Photonic Technologies (AIPT), Aston University, Birmingham, United Kingdom
[5] Unit of Urological Minimally Invasive and Robotic Surgery and Kidney Transplantation, Careggi University Hospital, Florence, Italy
[6] Department of Experimental and Clinical Medicine, University of Florence, Florence, Italy
[7] Unit of Gastroenterology, Careggi University Hospital, Florence, Italy
[8] Department of Biotechnology and Biosciences, University of Milano Bicocca and ISBE-Italy/SYSBIO, Milan, Italy
[9] LEONI Fiber Optics GmbH, 96524 Föritztal, Germany
[10] Modus Research and Innovation, Dundee, United Kingdom
[11] Department of Urology, Hospital Clinic, University of Barcelona, Barcelona, Spain
[12] Department of Physics, University of Florence, 50019 Sesto Fiorentino, Italy
[13] Laboratory of Photonics, Tampere University, Tampere, Finland

*These authors contributed equally
+Corresponding author: gustavo.castro@icfo.eu

Received xxxxxx
Accepted for publication xxxxxx
Published xxxxxx

## Abstract

For a long time, it has been known that optics can provide a broad range of tools for addressing clinical needs, particularly diagnostics. Optical techniques can help in identifying diseases and detecting pathological tissues with non/minimally invasive and label-free methods. Given the current limitations of standard clinical procedures, such an approach could provide a powerful tool in detecting gastrointestinal and bladder cancers. However, each technique has serious limitations regarding one or more of the following features: biomarker sensitivity, penetration depth, acquisition times, or adaptation to the clinical environment. Hence there is an increasing need for approaches and instruments based on the concept of multimodality; in this regard, we review the application of different imaging/spectroscopy tools and methods operating in the first two optical windows (SHG, SPEF, TPEF, THG, 3PEF, CARS, Raman and reflectance) for tumour detection in the digestive and urinary systems. This article also explores the possibility of exploiting the third bio-tissue transmission window (1600-1900 nm) by reviewing state of



 

**IOP** Publishing Journal Title
Journal **XX** (XXXX) XXXXXX https://doi.org/XXXX/XXXX

the art in ultrafast laser sources development. Finally, we summarise the most recent results in developing multiphoton endoscopes – a key element for clinical in vivo translation of photonics-based diagnostics.

Keywords: Label-free, cancer diagnostic, SHG, Raman, TPEF, microscopy.

## 1. Introduction and clinical needs

In 2020 more than 4 million cancer cases were diagnosed in Europe, and the most commonly diagnosed cancers were the following: breast, colorectal, prostate, lung and bladder cancers[1]. Compared to the 3.5 million cases from 2012, cancer incidence is clearly on the rise, and by 2040, the global number of new cancers per year is expected to rise to 29.5 million worldwide, including over 5 million in Europe alone[2,3]. Many risk factors contributed to such increase, including ageing populations, pollution, and occupational risks. Colorectal and bladder cancers experienced a particularly strong increase in their incidence rates, a trend that is likely to continue in the next decade. Thus, improvements in detection and treatments are greatly advocated[4–6]. The standard diagnostic test for detecting bladder tumours is white light imaging (WLI). However, this technique is burdened by false negatives and false positives at a non-negligible rate[7], as many endoscopic procedures can yield a high rate of false negative[8,9]. Other techniques require fluorescent labels, such as aminolevulinic acid or fluorescein, but are not routinely used in clinical practice, due to their high cost and marginal improvement concerning WLI[10,11].

In this framework, the introduction of new optical imaging techniques and related systems into the clinics have the potential to enhance the diagnostic power and the amplitude of their expanding biomedical applications, especially when implemented in a label-free modality. In fact, avoiding the administration of exogenous agents to the patient is a particularly crucial aspect for translating such promising technologies into clinical practice. For example, multimodal spectroscopy has already proved its potential in bladder cancer detection[12,13]. In addition, modern laser sources allow developing new imaging techniques[14,15] with the capability of reaching deeper areas of the examined tissue, avoiding tissue staining/labelling, potentially providing more information on the intrinsic content of the examined organs when compared to previous techniques.

A major obstacle to thoroughly appreciate current developments and future directions in this research area is the diverse nature of biological, clinical and technical challenges concurrently involved in tumour detection, as well as of these innovative technologies. Despite the relevance and interconnection of such topics, no attempt – to our knowledge – has been made to address them together in a comprehensive work. Therefore, given the rising interest for new optical methodologies and their possible application in the biomedical field, this article aims to provide an exhaustive review of the currently available label-free photonics-based techniques in cancer detection, with particular attention to those applied for urinary and colorectal cancers diagnostics. The information summarized in this work will hopefully help a broad range of clinicians and researchers in better understanding the capabilities and technical challenges of novel optical modalities and of the light sources involved in their use.

## 2. Current state-of-the-art of urological and gastrointestinal cancers detection

### *2.1 Clinically established techniques*

Current applications of optical techniques in urologic and gastrointestinal cancer diagnostics are many and different. The most clinically established techniques for urologic and gastrointestinal cancer are WLI, narrow-band imaging (NBI) and photodynamic diagnosis (PDD)[16,17]. WLI consists in shining a white light inside the patient through an endoscope or cystoscope. This well-established procedure helps doctors in visually assessing the presence of irregularities and suspicious areas. However, this technique provides small contrast for identifying specific types of bladder tumours, such as papillary lesions and carcinoma in situ hence causing higher recurrence-rates.

The further technical improvement led to NBI. NBI technology filters white light into two narrow bands (415 nm and 540 nm) that are efficiently absorbed by haemoglobin, increasing the visibility of surface capillaries and blood vessels in the submucosa. As carcinomas are highly vascularized, NBI enhances the contrast between superficial tumours and normal mucosa. Furthermore, studies conducted on bladder cancer have demonstrated that NBI is capable of detecting cancer areas more effectively than WLI[18,19]. In fact, the endoscopes/cystoscopes currently available with this technology allow switching from one narrow band to the other by simply pushing a button on the instrument. On the other hand, technical improvements were



 

also made in visualization and image enhancement, for example, Storz Professional Image Enhancement System (SPIES) have different visualization modules. Each visualization mode provides different colour contrast, which varies according to a clinical situation (i.e. haematuria) or surgeons' preferences[20], allowing better visualization of the mucosa than WLI in different modalities.

PDD consists of the intravesical administration of precursors of the heme biosynthesis pathway. In fact, protoporphyrin IX (PPIX), a precursor of heme, is photo-excitable with emission in the red when excited using 400 nm wavelength. Nevertheless, *in vitro* studies demonstrated that urothelial neoplasms have a higher intake of these drugs[21]. Another photosensitizing agent is the 5-Aminolevulinic Acid. This is captured by cells with increased metabolic activity and can be excited using blue light in the 375 to 440 nm range. The precursors, that absorb the excitation light, emit a red light, which provides a contrast enhancement compared to WLI. This technique was firstly reported by Höltl et al. (2001) as an experimental *in vivo* and *in vitro* treatment and has been proved to be viable and effective to highlight urothelial cancer during cystoscopy[22]. Subsequent studies reported good outcomes also in association with another photosensitizer, Hexaminolevulinate, which proved superior in detection rate to WLI[18]. However, the use of endogenous contrast agents does not allow this technique to be a routine technique; even in some cases, it is possible that contrast media are not used due to the risk of adverse reactions.

### *2.2 Alternative techniques in cancer detection*

Confocal laser endomicroscopy (CLE) is an optical imaging technique where a focused laser beam is scanning point by point to create a three-dimensional image; normally, a low-power blue laser for exciting fluorescence[23] is used. Exogenous fluorescence agents can be administrated either topically or systemically[24] to directly perform a pathological exam of the tissues without taking a biopsy[25,26]. This technique currently it is applied *in vivo*, especially in upper urinary tract urothelial cancer detection[26–28]. In a recently published systematic review and meta-analysis, CLE showed a good sensitivity and specificity in the detection of dysplasia in Barrett's oesophagus, gastric neoplasms and polyps, colorectal cancers in inflammatory bowel disease, malignant pancreatobiliary structures, and pancreatic cysts[29]. The main limitation of CLE is the fact that it needs for either topical or intravenous fluorescent agents. In addition to this, the technique is not widely available and need of specific training, it is of high cost and still there is a lack of comparison studies with other advanced optical techniques[23,29].

Autofluerence imaging (AFI) is another tool for cancer detection through fluorescence excitation. Differently from CLE, it doesn't use exogenous agents, hence a detailed description of its characteristics will be found in Section 3 among the other label-free techniques.

### *2.3 Unmet clinical needs*

Respect to WLI, the alternative technologies already available to clinicians do not provide – all things considered – the improvements required for replacing current gold standard procedures in the detection of urological /gastric tumours. Relatively high costs, low sensitivity to certain types of tumours, artefacts from exogenous agents, and operator-dependent analysis are the most important shortcomings that still affect the methodologies presented in this section. Therefore, there is still an unmet need for fast, reliable and economically sound systems to improve urothelial and gastrointestinal cancer management both for clinicians and for patients.

On the other hand, recent systems employing novel photonics-based technologies – multiphoton and spectroscopy imaging – are currently under development, and seems to provide good results *ex-vivo*[12–14]. These techniques can provide immediate, high contrast by analysing the intrinsic morphochemical content of tissues, especially when implemented in a multimodal approach. In this regard, the following sections will discuss the characteristics of label-free photonics-based techniques and their application to diagnosing cancer in both the digestive and urinary systems.

Currently available clinical techniques have different limitations. The lack of contrast makes the diagnosis strongly dependent on the clinicians' experience, which makes the results and interpretations susceptible to human error. On the other hand, although these techniques have shown great sensitivity in detecting cancer in its advanced stages, this has not been the case for early stages. The limited depth of penetration, as well as the need for not using contrast agents, has prompted research and the development of novel methodology and instruments for urologic and gastrointestinal cancers detection.

## 3. Emerging label-free optical techniques of urologic and gastrointestinal cancers detection

In the presence of incident light beam, several optical processes can occur at the same time. In inhomogeneous materials such as biological tissues, the different optical properties of each structure can produce different light-matter interactions, often resulting in different contrast mechanisms that can be exploited for tissue imaging. In this review, we have addressed 4 main

types of optical techniques in label-free modality: reflectance, autofluorescence, Raman spectroscopy, and multiphoton microscopy.

### *Optical reflectance*

Reflectance (elastic back scattering) is a simple and label-free technique that has been applied to both spectroscopy and imaging fields. A common implementation consists of illuminating the sample with a broadband source (e.g. a halogen or LED lamp) and collecting the reflected light. This approach allows investigating the scattering and absorption properties of the target and has been used for monitoring the presence of known absorbers within body tissues, such as haemoglobin, melanin and water[30]. WLI and NBI are clear examples of reflectance-based techniques.

### *Autofluorescence imaging (AFI)*

AFI has been recently developed to take advantage of the differences in tissue fluorescence properties of normal and neoplastic tissues that are generated by their endogenous fluorophores[31–34]. Narrow-band sources (such as lasers, diodes, and arc-lamps) can be used to excite endogenous autofluorescent molecules to higher energy states[35]. Biological tissues contain intrinsic fluorescent molecules, whose electronic transitions can be typically excited using UV or near-UV light: nicotinamide adenine dinucleotide (NADH), flavin adenine dinucleotide (FAD), collagen, elastin, lipo-pigments, porphyrins, etc[36,37]. Although fluorescent labels (such as the photosensitizing agents described in Section 2) are already used in the clinical practice, there are several advantages for adopting autofluorescence as label-free contrast mechanism for imaging biological tissues: the abundance of endogenous fluorophores and their relationship to metabolic activities, relatively high acquisition speed, and the possibility to use low-power light sources[38].

During cystoscopy, for example, normal tissue mucosa imaged with AFI typically shows a green colour, whereas an inflammatory or neoplastic lesion typically presents lower fluorescence intensity and appears brown-reddish or magenta. The potential detection efficacy of AFI for neoplasms lesion remains controversial though, as the use of UV or near UV limits diagnosis to only superficial layers, limited tissue samples have been studied to date, and a high level of skill is required, which may lead to misdiagnosis and low inter-observer agreement[39].

### *Raman spectroscopy*

The Raman signal can be used to identify both organic and inorganic molecules, opening a wide range of possible applications for industrial and clinical purposes. This is based on measuring the rotational-vibrational spectrum of a molecule, which is highly related to its geometry, especially in the so-called fingerprint region (300-1900 $cm^{-1}$). Therefore, a substance can be identified by observing its spectrum in such a region. There are two complementary optical techniques to do so: infrared (IR) absorption spectroscopy and Raman spectroscopy. The first is related to the interaction of IR light with the medium (absorption, emission or reflection) and in general, provides information on the vibrational states of matter. The latter is based on the Raman effect, i.e. the inelastic scattering of light after colliding with a molecule: the molecule undergoes a transition to a higher/lower rotational-vibrational energy state, causing the incident photon to lose/gain energy and to be scattered with a lower/higher frequency (Stokes/anti-Stokes Raman shift). Being independent of the excitation wavelength, this technique allows measuring the molecular rotational-vibrational transitions using either visible (380-700 nm) or NIR (700-2500 nm) laser light. However, the probability of Raman scattering is extremely low and, for biological tissues, the intensity of the Raman signal is several orders of magnitude smaller than the excited fluorescence emission. Consequently, the signal must be integrated for relatively long times, making such a technique typically used for imaging small areas. Nevertheless, the high specificity of Raman spectra has been successfully exploited for examining different body tissues, detecting and diagnosing many pathological conditions, including cancer[40,41].

### *Multiphoton microscopy*

Multiphoton microscopy (MPM) techniques refer to those generated by the interaction of two, three or more photons. MPM, being a nonlinear effect, requires high intensities to produce an efficient light matter interaction[15]. Therefore, focusing beam is needed, generating a nonlinear effect only at the focal region. In MPM the signal is collected with a detector while the laser is scanned through the sample (as in a confocal microscope). For this reason, such approach can produce high-resolution, three-dimensional images[14]. Among the main multiphoton effects used are: second harmonic generation (SHG), third harmonic generation (THG), two-photon excited fluorescence (TPEF), three-photon excited fluorescence (3PEF), and Coherent Anti-stokes Raman Scattering (CARS), as shown in Figure 1. Importantly, the efficiency of these nonlinear effects is based on their

intrinsic material properties. This has the advantage that no exogenous agents (e.g. fluorescent labels) have to be added to gain contrast. However, since these effects depend on the sample structure, not every effect can be generated from a particular sample.

### *Second harmonic generation (SHG)*

SHG is a process in which two incident photons are transformed into one photon with an energy that is exactly equal to the sum of the excitation photons. In this case, the SHG signal is generated only when the laser pulse interacts with a non-centrosymmetric structure. Collagen[42–44], microtubules[45,46], and myosin[47], among some others[44,45,48,49], exhibit this type of crystal symmetry.

### *Third harmonic generation (THG)*

THG is a process that requires three photons to generate one at an energy three times the excitation photons. THG depends on the inhomogeneity of the medium, which makes the THG interface sensitive. Therefore, it is possible to use the THG signal as a contrast mechanism to identify any cellular interface[50] where there is a strong change in the refractive index.

Importantly, both SHG and THG techniques provide useful and complementary structural information about the tissue without the need to use any exogenous agent. As such, they present a huge potential for use in diagnostic applications, although the excitation intensities required for their generation pose a higher risk of photodamaging tissues; this problem becomes more relevant as the nonlinearity of the optical process increases.

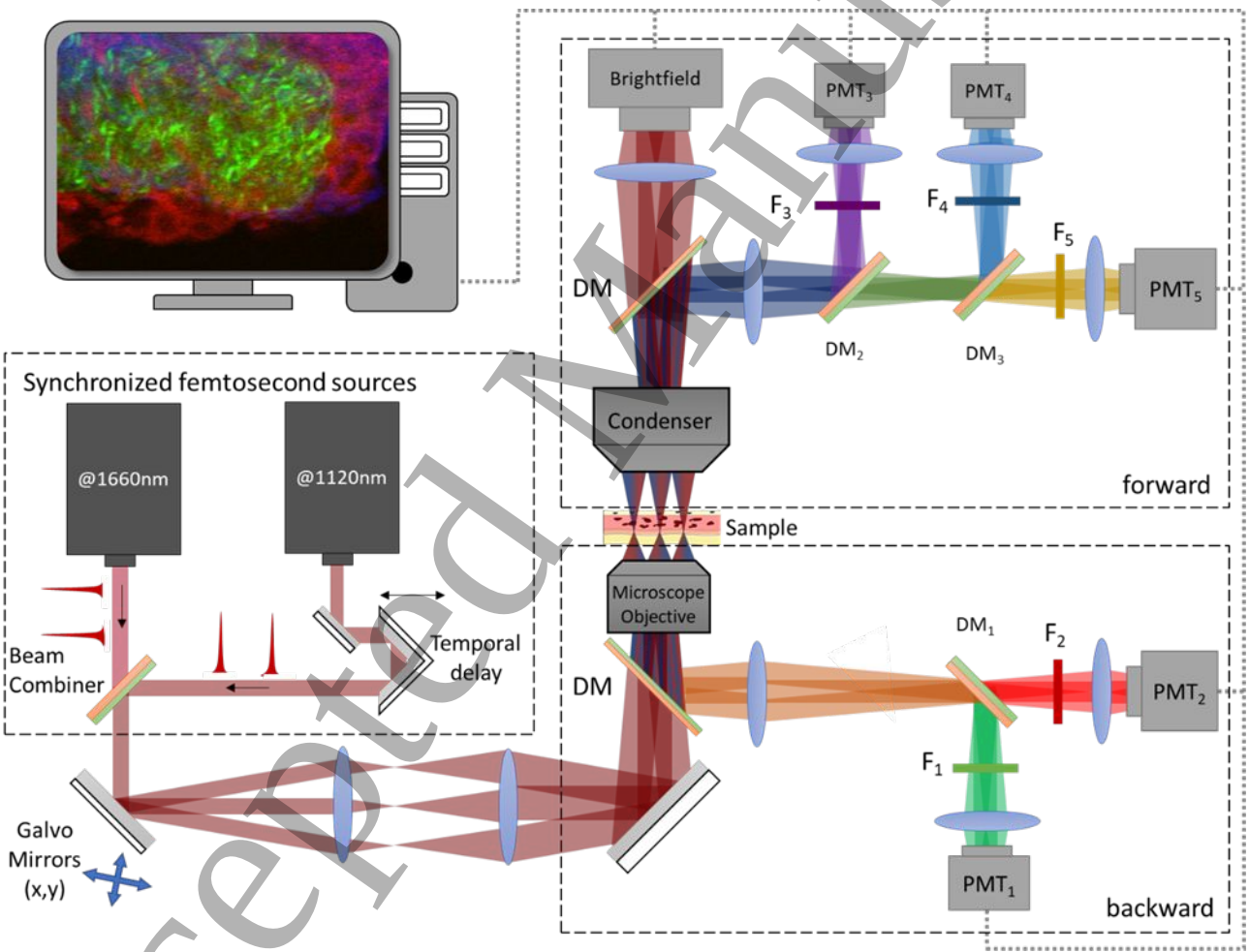


**Figure 1.** Schematic representation of a multiphoton microscopy setup. In a typical configuration, one or more pulsed laser sources emitting NIR wavelengths are linked to a scanning system and focused on the sample. Multiphoton-excited signals are then separated from laser path through dichroic mirrors (DM) and sent toward different photomultiplier detectors (PMT) equipped with specific optical filters (F). The detection system can be placed either backward or forward direction respect to sample position. Finally, multiphoton acquisitions are reconstructed via software and typically merged in pseudo-colour

images, highlighting the presence of different fluorophores or structures. With the correct selection of filters and dichroic mirrors, non-linear signals can be acquired simultaneously. For example, using a long-pass dichroic mirror at 1000 nm (DM) is possible split the beams from the excitation lasers from the non-lineal signals generated. In backward detection, using a long-pass dichroic mirror ($DM_1$) at 510 nm and two bandpass filters, one for a range of 450-500 nm ($f_1$) and the other for a range of 520-580 nm ($f_2$), it is possible to detect the 3-photon excitation autofluorescence signal induced with the 1120 nm laser from NADH ($PMT_1$) and FAD ($PMT_2$). In forward detection, using two long-pass dichroic mirrors, one at 500 nm ($DM_2$) and the other at 700 nm ($DM_3$), and three narrowband filters: 375 nm ($f_3$), 560 nm ($f_4$), and 845 nm ($f_5$), the THG ($PMT_3$), SHG ($PMT_4$), and CARS* ($PMT_5$) signals from the 1120 nm laser can be detected.

*CARS signal at 2906cm$^{-1}$ induced by the pump laser @1120nm and the stokes laser @1660nm.

### *Two- and three-photon excited fluorescence (TPEF, 3PEF)*

TPEF is a process in which a molecule is excited to a higher electronic state by absorbing two low-energy photons, rather than a single high-energy photon as in conventional fluorescence. After excitation, the molecule returns to its ground state by emitting a fluorescence photon, which has higher energy than the photons of the excitation light. Similarly, 3PEF is a process that consists of the simultaneous absorption of three incident photons, followed by the emission of fluorescence. Contrary to linear fluorescence, only a small volume around to the focal region is excited, reducing the photo-bleaching effect to only this volume. This considerably reduces the phototoxic effects and increases the viability of the sample. In addition, due to the wavelength-dependence of scattering, longer excitation wavelengths can penetrate deeper than shorter ones, even in highly dispersive media such as biological tissues[51–56]. Due to the wide availability of visible fluorescent biomarkers that can be excited using ultrashort pulsed sources, TPEF has become one of the most widely used nonlinear microscopy techniques, while there is growing interest in 3PEF applications (such as deep imaging of scattering tissues like brain[57,58]).

### *Coherent Raman scattering (CRS)*

CRS probes the same molecular transitions observable through spontaneous Raman spectroscopy, but in a much more efficient approach as it is based on stimulated emission. In fact, CRS techniques such as Coherent Anti-Stokes Raman scattering (CARS) and Stimulated Raman Scattering (SRS) need two synchronized lasers in order to induce a stimulated transition between rotational/vibrational levels, thus generating a signal which is orders of magnitude higher than the spontaneous process. In SRS, the target molecule is excited from the initial state toward a nearby rotational/vibrational level by two incident photons (a "pump" and a "Stokes" one), whose energy difference matches the separation between those levels. During such process, the SRS effect can be observed via changes in the Stokes beam intensity. Compared to SRS, in CARS the molecule is further excited toward a virtual level using another pump photon ("probe"), and then the molecule relaxes to its ground state emitting a high-frequency photon – the CARS signal to be detected. These two CRS techniques can be used for label-free imaging based on specific Raman bands (typically) of lipids and proteins.

## 4. Advanced imaging technologies for cancer detection

### *4.1 Applications to cancer detection in the gastrointestinal system*

During the 1990s, studies on this subject involving autofluorescence[59–62] and optical reflectance tecniques[63,64] were published, showing their potential. During the 2000s, studies based on Raman spectroscopy[65–67] were also presented. A literature review (Tables A1[59–62,68–75], Table A2[63,75–85] and Table A3[65–67,73,86–94] in the Annex section) suggests that these techniques could be successfully applied – both *in vivo* (through endoscopy) and *ex-vivo* – to the detection of gastrointestinal tumours. The research on the field continues to the present day.

A consensus is that neoplastic tissues in the gastrointestinal system are characterised by both lower absolute intensities in fluorescence emission and higher red-to-green ratio with respect to non-tumour areas[68,71,75,95–97]. In fact, several factors have been cited to explain these effects in tumours: bigger cells, causing a reduction in collagen and elastin concentrations (which contribute to green fluorescent emission); thicker mucosa layer, screening off collagen/elastin emissions from the submucosa layer; higher concentration of non-fluorescent NAD+ relative to fluorescent NADH; increased concentration of red-emitting porphyrins. Such features usually provide high sensitivity on average (~90%) in tumour detection, although there is great variability in reported sensitivities (Table A1).

Another feature observed in a gastrointestinal tumour is angiogenesis, where resulting hypoxia and increased haemoglobin concentration can be probed through reflectance measurements[63,81,84,85]. Moreover, several studies[75,77,79,82–85] obtained better

sensitivities and specificities by extending the analysis to longer wavelengths, above 900 nm, where fat, collagen and water are important chromophores. On average, the presented studies on reflectance-based endoscopy (Table A2) obtained ~90% sensitivity and specificity.

Raman systems (mainly fiber-optic probes) were applied to study gastrointestinal tumours, providing important insights on the molecular composition and metabolic activity of such tissues. The analysis of tumour Raman spectra highlighted a reduction in glycogen[65,98], collagen and lipids concentrations[87,88], together with an increase in DNA contents[86,90]. These findings are consistent with hallmarks of tumour development, including increased energy consumption from cell division, increased thickness of the gastric epithelial layer due to proliferation of the malignant cells and increased nuclear/cytoplasmic ratio. Almost all the studies reported in Table A3 used NIR wavelengths and adopted supervised learning algorithms to differentiate tumour from non-tumour tissues with high sensitivity and specificity. Importantly, half of the studies reported in Table A3 performed *in vivo* measurements, paving the way for clinical implementation, preferably in combination with the other two techniques.

In the digestive system, multiple research groups have focused on gastrointestinal cancer detection using non-linear optical methods, including SHG, THG, TPEF, 3PEF, CARS and SRS (Table A4). Many focused their efforts on detecting SHG produced by collagen[51,99–112]. As a result of these investigations, healthy and cancerous tissue can now be distinguished based on histological differences, using THG to distinguish the boundaries of different biological components (tissues, cells or cellular components)[113,114]. Furthermore, autofluorescence has been used to identify the signals and distribution of FAD and NADH into the tissue using TPEF or 3PEF[51,103,110,112]. Recently, this has been used to generate multiphoton images with a resolution comparable to histopathology[43,108–114]. Nonlinear microscopy has proven to be a useful imaging tool for the qualitative and quantitative evaluation of various diseases. Furthermore, due to the nature of non-linear signals, it is possible to collect simultaneously structural (SHG, THG) and metabolic (TPEF, SRS, CARS) information from the tissue. All of this can be done with minimal phototoxicity to tissues, at depths of several hundred microns with the ability to detect cellular and subcellular microstructures of tissues[108,111,112]. Due to these advantages, some research groups have focused on gastrointestinal cancer detection using multiphoton techniques. Most of these investigations use biopsies from different parts of the gastrointestinal tract. However, some investigations have taken these techniques to an intraoperative level and have been able to distinguish between healthy tissue and gastric carcinoma *in-situ* and *in vivo*[51,99,100,113].

### *4.2 Applications to cancer detection in the urinary system*

During the 1990s, several studies investigated the possibility of using tissue autofluorescence for detecting bladder tumours, beginning with *in vivo* measurements through a bifurcated fiber-bundle inserted into a cystoscope (Figure 2), observing that tumour areas show an average decrease in NADH and collagen fluorescence intensity with respect to normal bladder mucosa[115]. Later studies, for both *in vivo*[116–119] and *ex vivo*[120,121], adopted similar approaches (based on fiber-optic probes) and confirmed these results. Moreover, tryptophan, FAD and porphyrins were found to be other major fluorophores involved, and UV excitation wavelengths (<400 nm) were found to be more effective[120,121] in discriminating normal and tumour tissues. Finally, the research suggested that collagen and NADH emissions are reduced by thickening the urothelial layer in tumours[120,121], which prevents the detection of autofluorescence coming from deeper layers (i.e. from collagen in the lamina propria and NADH in muscle layers).

The observed spectral changes, including a spectral redshift in tumour peak intensity[12,13,118], were used for discriminating neoplastic tissues from the normal bladder. The most common approach consisted in calculating the ratio between fluorescence intensities detected at two separated wavelengths, but two studies[12,13] adopted a method based on Principal Component Analysis (PCA), a well-known statistical tool for multivariate analysis. Table A5 summarises the major findings of the above-mentioned studies. Tumours were detected on average with ~90% sensitivity and specificity, despite variation from differing experimental conditions (number of patients and samples, excitation wavelength, data analysis, instrumentation, etc). Hence, autofluorescence spectroscopy appears as an effective tool for improving the detection of bladder tumours during cystoscopy.

*In vivo* studies[122,123] examined bladder tumours through another technique: reflectance spectroscopy. Using broadband excitation sources (such as halogen or xenon lamps) and collecting the reflected light upon large spectral ranges (~hundreds of nm), normal and neoplastic tissues' absorption and scattering properties were investigated. Mourant et al. (1995)[122] developed a classification method based on the spectral slope recorded in the 330-370 nm range. Koenig et al. (1998)[123] analysed longer wavelengths to probe the total amount of haemoglobin (hence, of blood), which they found to be higher in tumours. This finding was also observed by Slaton et al. (2016)[124], and appears to reflect tumour angiogenesis, i.e. a higher microvessel density in neoplastic tissues with respect to the healthy bladder. Such features were later exploited for the implementation of Narrow Band Imaging (NBI) in bladder tumour detection. By filtering both excitations and reflected light signals within two narrow

bands, centred on major haemoglobin absorption peaks (415 nm and 540 nm), it is possible to enhance the contrast between well-vascularized lesions and normal mucosa. This technique can be implemented in video cystoscopes and used for real-time imaging of the bladder. For example, Rosenzweig et al. (2018)[125] listed 12 in vivo studies comparing NBI to standard white-light cystoscopy, of whom we included in Table A6 those with >100 patients[126–129]. Another feature for differentiating normal bladder from cancer may be the slope of reflectance spectra recorded between 600 and 700 nm [13]: being proportional to the average size of light scatterers, such parameter could highlight the presence of tumour cell nuclei, as (on average) they are bigger than normal ones.

In general, tumour identification through reflectance-based methods is characterised by high sensitivity (up to 100%), whereas specificity values fluctuate mostly between 60% and 80%. However, results from spectroscopic[12,13,122–124] and NBI studies are difficult to be compared: the former is based on objective parameters extracted from the spectra, while the latter are based on "the physician's ability to identify tumours as well as to other subjective factors"[129]. Another important difference between the two approaches is that fiber-optic devices used in spectroscopy require scanning the probe along with each point of the examined tissue area, whereas all pixels of the NBI image are recorded simultaneously, allowing faster acquisitions.

Both fluorescence and reflectance have been successfully employed for detecting intrinsic differences in the composition of benign and malignant bladder areas. In this regard, Raman spectroscopy could provide an additional and more detailed characterisation, being able to probe molecular content of these tissues. The first attempts came in the early 2000s from Stone et al. (2002)[65] and Crow et al. (2004)[130], with both groups obtaining very high sensitivity (>97%) and specificity (>93%) in

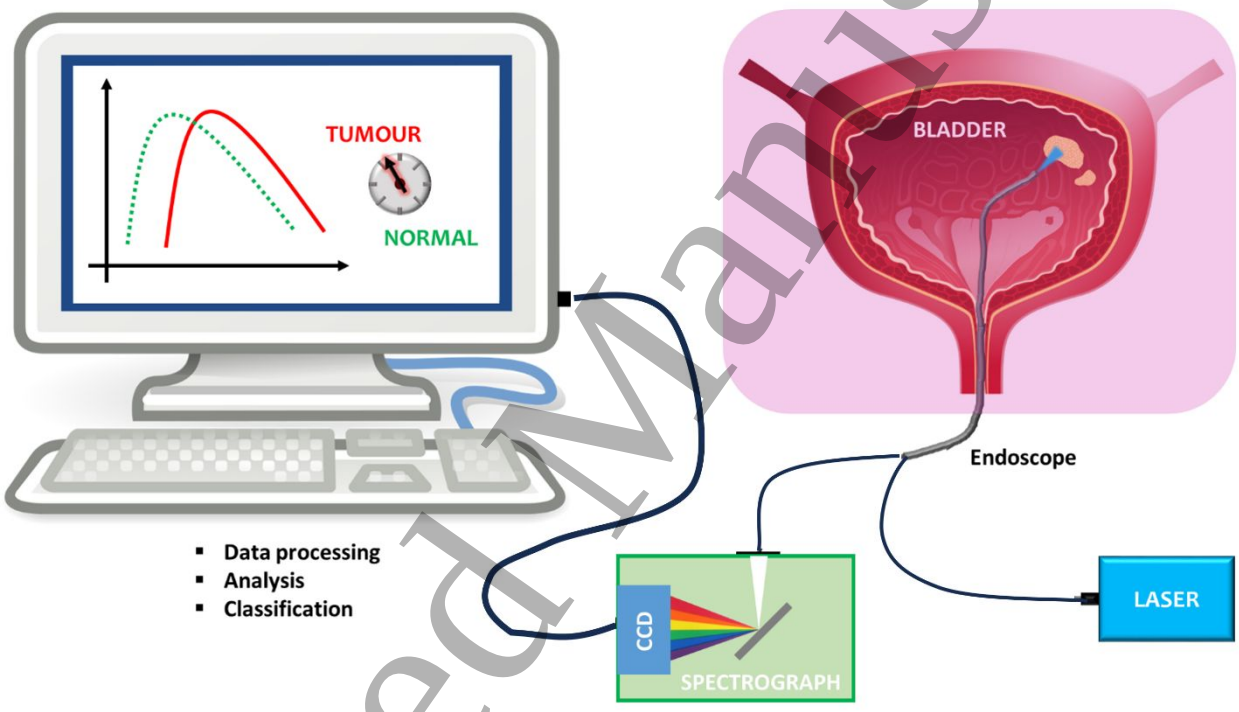


**Figure 2**. Schematic representation of a fiber-probe endoscope for bladder cancer detection. The probe is connected both to an excitation source and a detection system (typically consisting of a spectrograph and a CCD). The signal collected from suspicious tissue areas is processed and analysed – often through supervised-learning techniques – in order to be classified as either healthy bladder mucosa or urothelial carcinoma.

discriminating bladder cancer. These studies paved the way for developing and applying Raman fiber-optic probes to the same biomedical problem, resulting in many independent papers[12,13,131–136] that validated the previous results. Table A7 lists the Raman literature on the field. Most of the reported works shares common features, such as employing fiber-probes, adopting NIR excitation wavelengths (785 nm being the most common), and analysing the recorded dataset through a combination of PCA and linear classification models (mainly Linear Discriminant Analysis). Moreover, there is general agreement about the interpretation of Raman spectra: compared to healthy mucosa, decreasing collagen content and an increasing presence of lipids, amino acids and DNA were observed in cancer spectra[12,132,134,135,137], reflecting the altered metabolism of tumour tissues.

On average, Raman spectroscopy/microscopy obtained ~90% sensitivity and specificity in detecting bladder tumours. Notably, there is smaller variability between the results of Raman papers than among the fluorescence literature on the same subject. However, all but one[132] of the studies reported in Table A7 were conducted *ex-vivo*. In fact, the main challenge in using Raman-based methods is their relatively long integration time: recording a spectrum typically required 10-20 seconds in the reported literature, which is several orders of magnitude higher than in fluorescence/reflectance-based techniques. This is a clear obstacle for *in vivo* implementation in the clinical setting.

On the other hand, Raman spectroscopy has also been applied for differentiating bladder tumour grades (Table A8) by exploiting its higher molecular specificity with respect to other techniques. Such a task can be performed after tissue excision, hence measurements requiring a few tens of seconds or minutes would pose no effective delay nor an obstacle to standard clinical routines. The known literature reports 89% sensitivity and 83% specificity, on average, in discriminating low-grade (LG) from high-grade (HG) bladder tumours. Efforts were also made to differentiate bladder tumour stages, such as $T_a$ (non-invasive), $T_1$ (connective-tissue-invading) and $T_2$ (muscle-invading) urothelial carcinomas[12,13,130,132]. The results obtained in differentiating $T_a$ from the two invasive stages range between 96% sensitivity / 96% specificity obtained in Crow et al. (2004)[130] and 41% sensitivity / 83% specificity in R.O.P. Draga et al. (2010)[132]. Raman spectroscopy could play an important role in examining freshly excised tissue biopsies and providing an automated diagnosis of bladder tumours, which would help in designing a proper medical treatment immediately after cystoscopy.

As with gastrointestinal cancer, ongoing work uses MPM to detect bladder cancer (Table A9[140–145]). To date, most applications using MPM are limited to biopsies. There are various approaches to collecting and discerning this information. The most explored way is collecting the SHG produced by collagen fibers. By comparing collagen fibers morphology, several studies have been able to differentiate between healthy bladder tissue and carcinoma[140–146]. It is also possible to take advantage of the information of autofluorescence induced by the absorption of two or three photons of molecules whose absorption is in the UV region including NADH, keratins, melanin, and elastin. Since these techniques induce the fluorescence of endogenous tissue molecules, different spectral analyses can be incorporated into the signals in order to differentiate the molecules. One approach is to fix the sources of ultrashort pulses to the most efficient wavelength for each of the endogenous molecules and generate maps of the different signals of the tissue. It is also possible to combine nonlinear techniques with techniques based on fluorescence lifetime, such as Fluorescence lifetime imaging Lifetime Imaging Microscopy (FLIM) or Spectral fluorescence Lifetime Imaging Microscopy (SLIM) to differentiate each endogenous molecules of the tissue[12,141,143]. With this, it has been possible to determine the distribution of the FAD and NADH molecules. In addition to this, with the structural information obtained by SHG collagen, notable differences have been demonstrated between the regions of healthy tissue and urothelial carcinoma[12,140–143].

As previously mentioned, many studies have identified Raman spectrum peaks where there is greater variation between healthy tissue and urothelial carcinoma. They have taken advantage of Raman information to generate metabolic maps through the use of techniques such as CARS or SRS. Finally, there are more ambitious works that have managed to collect simultaneously the signal of TPEF, SHG and CARS and combine this information with the spectral information from TPEF-FLIM and Raman[144] to generate multimodal images contrasting morphological and metabolic characteristics between healthy tissue and cancer. Thus, research has demonstrated the ability of these modalities to provide diagnostic information, and their potential to become a diagnostic tool for detecting the disease in its early stages and improving the understanding of associated pathophysiological processes.

### *4.3 Laser sources for optical diagnostics of the digestive and urinary systems*

Optical reflectance techniques for tissue classification typically require the use of broadband light sources and optical filters in the emission and collection light paths.. Fluorescence or Raman generation, instead, requires narrow-band, continuous wave (CW) laser sources, the most popular[147,148] being semiconductor laser diodes.

Diverse categories of pulsed laser sources are used for the optimal functioning of multiphoton microscopy (MPM) systems, contingent upon their specific applications. Consequently, determining the most suitable excitation light source for MPM of specific tissue types presents a complex challenge. Multiple parameters warrant consideration for an effective comparison, including but not limited to: image quality (comprising both blur and noise), sample safety, imaging depth, and the versatility of available imaging modes, etc[149]. Figure 3 depicts the emission wavelength ranges that most of the commercial lasers[150,151].

Solid-state lasers employ a crystal or glass host material that is doped with specific ions such as Neodymium (Nd), Ytterbium (Yb), Chromium (Cr), or Titanium (Ti) to achieve the desired lasing wavelength. These lasers can operate across a broad spectrum, ranging from the visible to the near-infrared, typically between 0.5 and 1.6 μm[152]. Semiconductor lasers function

across an extensive wavelength spectrum, from ultraviolet (UV) to mid-infrared (MIR), partially encompassing the biological windows except for the third one. InGaAs, with a tunable direct bandgap, is ideal for specific wavelengths in biological windows, while GaAs is used for near-infrared lasers and AlGaInAsSb for lasers beyond 2 μm in the mid-infrared range[150]. In fiber lasers the active gain medium is doped with rare-earth elements such as Erbium (Er), Ytterbium (Yb), Thulium (Tm) and etc[151]. The operational wavelength range of fiber lasers is generally between 1 μm and 2.2 μm, although specialized designs and methods can extend this range. One such method is supercontinuum generation, which is produced by the propagation of intense laser pulses in a transparent nonlinear medium, resulting in ultra-broadband radiation. This radiation has a high power spectral density and a high degree of coherence, making it equivalent to a white-light laser[153].

In the context of MPM, the most used and explored source is the titanium-doped sapphire (Ti:Sapphire or ti:sapph)) laser,as this can be used to excite nonlinearly most of the visible fluorescent markers. A high saturation energy, large stimulated emission cross-section, and broad absorption gain bandwidth make Ti:Sapphire the most successful solid-state laser material in the near-infrared (NIR) wavelength range. They have excellent tunability in the range of 650-1100 nm and high potential for ultrashort pulses creation.

However, Ti:Sapphire lasers are generally confined to the laboratory. These lasers are not appropriate for industrial or mobile applications due to their temperature and vibration sensitivity. Furthermore, they are still massive, complex, high-priced[151]. In this context, cutting-edge fiber lasers are excellent alternative which could offer compactness, industrial reliability, power scalability, wide spectral working range and superior beam quality from the fiber output[154].

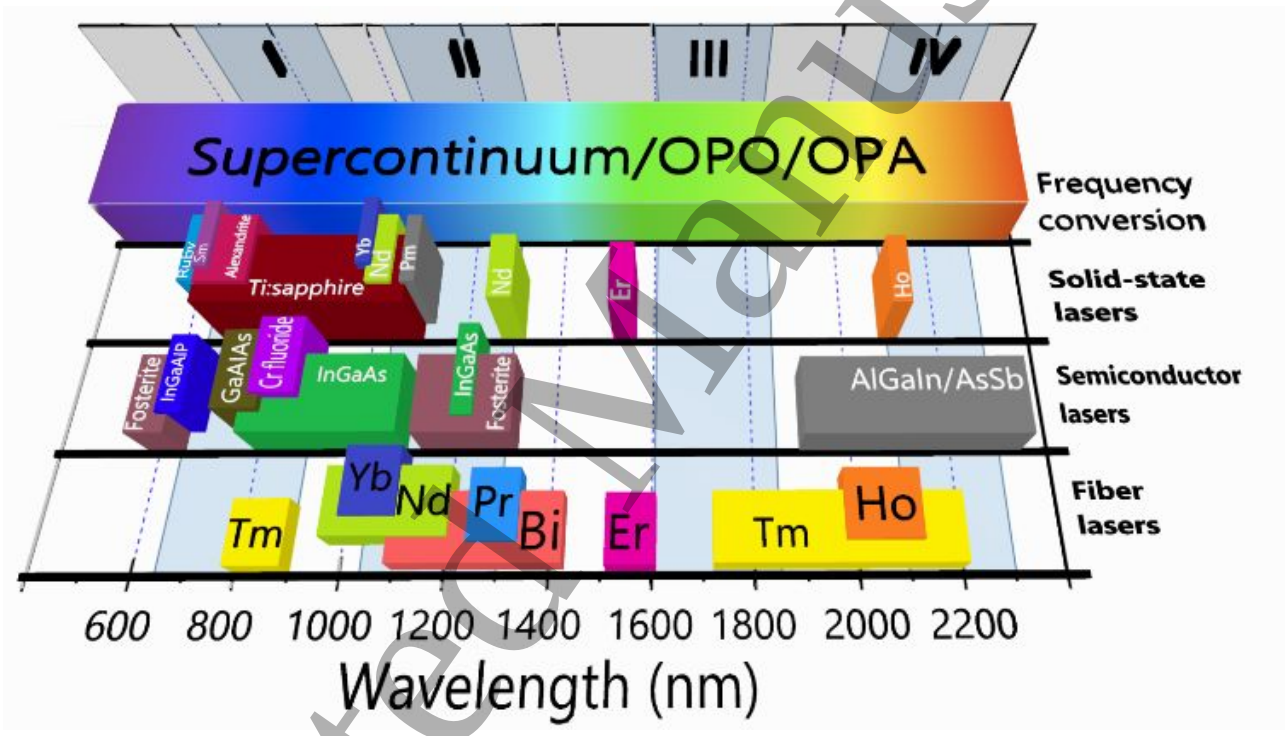


**Figure 3.** Commercially available laser sources operating within biologically wavelength ranges.

## 5. Complementary technologies for in vivo detection of bladder and gastrointestinal cancers and future

### *5.1 Multimodal Multiphoton Micro-endoscopes*

*In vivo* implementation of multiphoton techniques – especially in a multimodal configuration – offers a promising tool for assessing the presence, grade and stage of tissue lesions like bladder/gastric tumours. Such task is currently carried out *ex-vivo,* i.e. through biopsy extraction and histopathological examination, but this procedure has some limitations: high cost, invasiveness, sampling errors, time-consumption and the inability to monitor the lesion. Multimodal Multiphoton Microscopy (MMM), on the other hand, could provide label-free, high-resolution optical sections of a few hundred micrometres below the

tissue surface, without the need for collecting and staining biopsies, providing high-sensitivity 3D images with micrometre accuracy. Moreover, MMM could also be used for better defining tumour margins during surgical removal. However, the greatest challenge in the clinical translation of this technology is the difficulty in obtaining multiphoton images from internal organs, which requires the development of fully integrated multimodal microendoscopy systems (Tables A10 and A11[155–169]).

Currently, microendoscopy systems have been able to be fully integrated into probes of 3 mm in diameter and 4 cm in length[155-157] to satisfy the clinical requirements for use at the hospital level. These probes are made up of microelectromechanical mirrors or piezoelectric actuators[158], to control the position of the excitation laser. Furthermore, these probes are coupled to double-coated optical fibers[155–163], which allows the excitation and emission wavelengths to be transmitted efficiently.

However, translating multimodal microendoscopy to the clinic involves many technological challenges. It is essential that the microendoscope is small enough (i.e., less than 2mm in diameter) to be inserted into a clinical endoscope[159–161]. Furthermore, for efficient multiphoton excitation it is necessary to deliver ultrashort IR pulses thorough to several meters long of optical fiber, with efficient dispersion management to ensure high peak powers at the end of the endoscope and without introducing distortions[164–169], whilst keeping the large field of view (FOV>150 μm), the large working distance (WD>1 mm) and the highest resolution possible (<1 μm). The development of this technology has been increasing progressively in recent years, making pulse transmission and detection more efficient. These advances in multimodal endoscopic imaging capabilities present numerous promising opportunities for applications in both clinical diagnostics and basic research, creating a tool for real-time gastrointestinal and bladder cancer diagnosis and treatment.

### *5.2 New technologies for deep tissue multiphoton imaging*

To increase tissue penetration depth, efforts have been focused on using longer wavelengths, where scattering is minimized. Additionally, due to the high peak intensities required by the non-linear process, it is necessary to work in the so-called biological windows, where light absorption is minimal. Currently, there are four known wavelength regions, or biological windows[170], listed in Table 1. Each biological window has a different transmission depending on the specific biological tissue[15,155].

**Table 1.** The list of biological windows. The bandwidth of each biological window is listed in the second column from the left. The wavelengths of nonlinear excitation (third column) and the generated signals for the case of SHG and THG are listed in the third and fourth columns, respectively.

| Biological window | Wavelength range [nm] | Fundamental [nm] | SHG [nm] | THG [nm] |
|---|---|---|---|---|
| 1st | 700–950 | 825 | 412 | 275 |
| 2nd | 1000-1350 | 1150 | 575 | 383 |
| 3rd | 1600–1870 | 1700 | 850 | 566 |
| 4th | 2100–2300 | 2200 | 1100 | 733 |

In biological terms one of the advantages of the ti:sapph laser is the most works in the first biological windows. Nevertheless, the generated nonlinear signal (TPEF, SHG, THG, etc.) are generated in the visible, far from an biological window. This will limit again the sample depth that can be examined through these techniques, as optical scattering will further reduce the intensity of the collected nonlinearly generated signal. On the other hand, the second biological window is being explored more and more due to the different commercially available laser sources (Ytterbium (Yb)-based laser). However, the non-linear signals are also produced in the visible range. Despite recent advancements in Tm and Ho ultrafast laser sources, the fourth biological window (2100 to 2300 nm) has been largely ignored. This is primarily due to the high water absorption in this wavelength range and the lack of high-sensitivity imaging detectors suitable for these wavelengths[171–175].

The potential of the third wavelength range of the biological window (1600-1870 nm) in multiphoton imaging remains largely unexplored, but it promises several advantages for working with deep tissues compared to the first and second transparency windows. Studies using 1700 nm excitation have demonstrated deep brain imaging experiments (signal-to-noise ratio (SNR) of ~5 dB) and a penetration depth of 1.1 mm[176]. Similar results have been achieved in the urinary system, with a 1700 nm light source reaching a penetration depth of ~800 μm in normal prostate tissue[177]. As mentioned, the scattering decrease as the excitation wavelength increases. This means that less power is needed to reach the focus with longer-wavelength light, significantly increasing the penetration depth in tissues[176]. Additionally, the nonlinear features of multi-photon

microscopy allow for minimizing out-of-focus light excitation and photobleaching of biological samples[178]. Considering the increased penetration depth and reduced effect of optical scattering, the use of these longer wavelengths for both excitation and emission are highly favorable for imaging systems[14]. Therefore, one of the most interesting regions is the third biological window; however, there are still no commercial femtosecond lasers in this region.

In this review, we focus on the two most popular techniques to achieve pulsed laser radiation in the 3rd biological window: optical parametric generators and pulsed fiber lasers.

### *Optical parametric generators and amplifiers*

One of the most popular methods for generating laser sources emitting radiation in the third biological window is optical parametric generation. his approach offers a wide range of precisely tunable wavelengths with a high signal-to-noise ratio (SNR), making it suitable for many applications including bio-imaging, time-resolved spectroscopy, chemical sensing, and microscopy[179–181]. Parametric light generation relies on the phenomenon where an incident photon in a nonlinear optical medium converts into two lower-energy photons, called the signal and idler waves. Their wavelengths are determined by the phase-matching condition and the principle of energy conservation. Phase-matching conditions can be changed by media temperature or, in bulk optics, by the angle between the incident pump beam and the crystal optical axes.

As a pump source, optical parametric oscillators (OPOs) are the primary approach of optical parametrical light generation. Here, a nonlinear medium is placed in the cavity and the signal and the idler waves are built up from the noise using pump wave and cavity feedback (Fig. 4)[182]. O'Connor et al. (2002) reported a synchronously pumped, periodically poled lithium niobate-based OPO with signal output tuned from 1550 to 1950 nm[183], obtaining up to 90 mW average power in a signal wave.

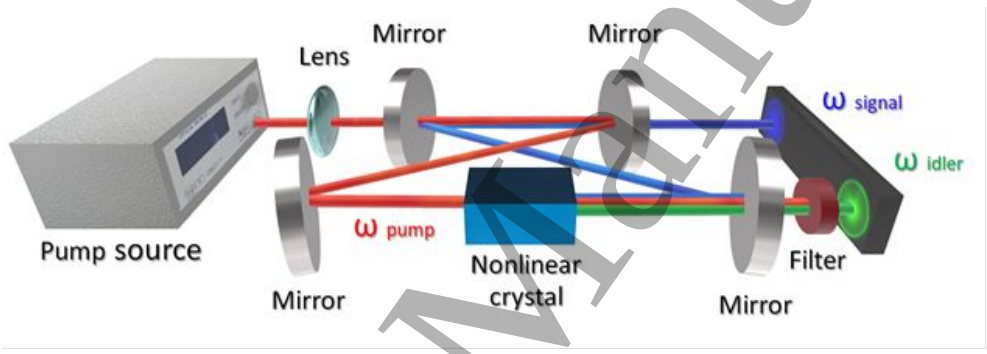


**Figure 4.** Schematic diagram of OPO based source.

To increase the output power and improve the conversion efficiency, an optical parametric amplifier (OPA) with a low-power seed source is commonly used. OPOs acting as a seed source are widely applied in the OPA based sources of third biological window radiation[184]. For instance, Morz et al. (2015) have demonstrated an optical parametric MOPA, tunable from 1370 to 4120 nm [185]. For pumping, a Yb:KGW laser was used, which delivers up to 8W average output power at 43MHz repetition rate and 500 fs pulse duration at a central wavelength of 1030 nm. OPO and OPA were based on periodically-poled magnesium oxide doped congruent lithium niobate crystals. This system allows obtaining a high average power of up to 1.3W at 1750 nm with 43 MHz repetition rate. OPO seed sources provide high pulse-to-pulse stability and SNR which positively affects bio-imaging. However, they have complex optical schemes and highly precision alignment requirements. To avoid these issues, SC sources are often used as an OPA seed[181,186–188]. Optical parametric systems allow obtaining required laser radiation parameters at the third biological window, and they are capable of satisfying high requirements of bio-imaging but usually have a high cost, large footprint, and sensitivity to vibration. In fiber parametric oscillators (FOPO), these disadvantages are partially eliminated. Becheker et al. (2018) demonstrated all fiber FOPO laser system at 1700 nm [189], obtaining 14.3 mW average power at 1700 nm. Power scaling in the FOPO system can be very difficult due to the nonlinear effects in optical fiber, keeping the output power less than 20 mW. To increase the output power, it is necessary to use optical parametric chirped-pulse amplifiers (OPCPA)[190], which allows pulse amplification greater than 25 dB at 1550 nm [191]. With the correct fulfilment of the phase-matching condition, this approach makes it possible to get a wide-range wavelength-tunable fiber laser at 1700 nm [192]. Recently, a laser with a 450 fs pulse duration at 1700 nm and an average power of 1.41 W has been developed[193]. However, it features an extremely complex tuning mechanism and requires the use of specialized fibers. Well-known methods widely employ

specialized fibers such as photonic crystal fibers, dispersion-shifted fibers (DSF), or highly nonlinear fibers (HNLF) for wavelength conversion and energy scaling purposes.

The OPO and OPA systems are attractive for bio-imaging due to high SNR and pulse-to-pulse stability. On the other hand, fiber lasers are great at working in harsh environments.

*Ultra-short pulsed fiber lasers*

The development of a highly stable, robust, compact, easy-to-use, and more affordable ultrashort pulse fiber laser has opened the door for multiphoton microscopy systems to be used in the clinical environment. The ultrafast rare-earth-doped fiber lasers are highly adaptable and more compact than many of their counterparts. Furthermore, they offer simplicity of exploitation and reliability at working in harsh and inhospitable environments. Despite the fiber medium of lasers, the repetition rate of ultrashort fiber lasers could be adjusted in order to applications requirement by acousto-optic[194], applying piezo elements[195] or harmonic mode-locking methods[196,197] with optical injection[198].

Recently, bismuth (Bi)-doped fibers have become popular as an active media of lasers. The main reason is the discovery of a broadband luminescence in the near IR region (1100-1800) nm in several Bi-doped glasses (silicate, germanate, aluminophosphate, barium-aluminoborate). The unique optical properties of Bi-doped fibers provide an opportunity to generate laser pulses in the broad spectral regions for various applications[199–203].

Using a high concentration of $GeO_2$ and $SiO_2$ in a Bi-doped fiber core, the emission spectral range could be extended to the wavelength region from 1.6 to 1.8 μm [202]. The first 1.7 μm Bi-doped fiber laser generating ultrashort pulses via passive mode-locking was demonstrated by Noronen et al. in 2016[203]. Later, the 630 fs pulse and output pulse energy of 5.7 nJ at 1.7 μm were achieved in the Bi-doped fiber master oscillator power amplifier (MOPA) by Khegai et al. (2018)[199]. Bi-doped fibers are an immature technology though and have a small core diameter (~ 2 μm), which leads to low pulse energy at the output and a requirement for a large cavity length due to the low gain per meter. The usage of Bi-doped fibers limits the fundamental pulse repetition rate up to 10 MHz in such lasers[202,203].

Thulium (Tm)-doped fiber lasers operating at a wavelength of 1700 nm and longer, are more efficient than lasers based on Bi-doped fibers. A higher doping level of Tm in optical fibers allows shortening the cavity length and attaining higher energies. To investigate the expanding range of radiation tuning (1788-1831 nm and 1702-1764 nm) in a mode-locked fiber laser doped with Tm, Emami et al. employed a specially designed photonic crystal fiber (PCF)[204]. By relying on the partial amplified spontaneous emission suppression mechanism, which involved the combined use of two fabricated PCFs and the nonlinear polarization rotation method, the laser's emission wavelength band was effectively tuned. Advancements in the production of high-performance Tm-doped fibers enabled the development of a mode-locked fiber laser capable of generating ultrashort pulses in the wavelength range of 1700-1900 nm. Utilizing an acousto-optical filter allowed for effective control of the spectral range within the cavity. The laser, combined with a Tm-doped fiber amplifier, produced pulses at 1708 nm with an energy of 1.85 nJ [205]. Nevertheless, the strong reabsorption at 1700 nm in Tm-doped fibers makes reaching high-performance laser sources at the shorter wavelengths highly difficult.

Erbium-doped fiber (EDF) has become the central component of nearly all optical amplifiers in the 1500-1600 nm spectral region. The most developed laser systems operating in this region are based on EDF, as EDF provides an efficient broad-band gain in the telecommunications window. The amplified spontaneous emission bandwidth of EDF does not cover the third optical window, although nonlinear effects in optical fibers can provide a frequency shift of EDF lasers. The self-phase modulation (SPM)[206] and cross-phase modulation[207], four-wave mixing[208], stimulated Raman scattering (SRS)[209,210], and stimulated Brillouin scattering[211,212] are all to play important roles in the creation of fiber lasers and amplifiers, signal format conversion and wavelength conversion devices[213]. These nonlinear effects are actively used in optical fibers to shift the spectral envelope of the pulse or generate new frequency components, including the generation of radiation in the third biological window.

Currently, several technologies are actively used to transfer energy from the Erbium emission wavelength (1500-1600 nm) to the range of the third biological window 1600-1870 nm, based on nonlinear effects in optical fiber. Xin He et al. (2019) demonstrated a compact laser with a pulse width of 384 fs and an average power of 35 mW with a conversion efficiency of about 60% using 460-meter of standard single mode (SM) fiber telecom for a frequency shift of up to 1700 nm [214]. ZDW-shifted fibers are frequently employed in the implementation of both SPM and SSFS techniques, with the objective of attaining wavelengths in the range of 1650-1750 nm [215,216].

Cadroas et al. (2017) endeavored to enhance the output characteristics of radiation by devising a specialized fiber possessing a LMA. In conjunction with a cladding mode stripper and a band-pass filter employing soliton self-frequency shift, they achieved pulses with a 9 nJ energy, 75 fs duration, and a wavelength of 1650 nm [217]. Subsequent studies employing commercially available LMA fibers have demonstrated comparable conversion efficiencies[218]. In 2014 K. Wang et al. presented the SSFS system based on photonic crystal rod (PC Rod) that could prove the pulse with energy >60 nJ [219]. However, they

require much higher initial pump pulse energy, water cooling, and cannot be coiled. The progress in developing tunable ultra-short fiber pulsed lasers covering the third biological window gives the ability to choose the most appropriate laser parameters for deep and high-resolution imaging. Table 2 demonstrates the results achieved in generating ultrashort laser pulses at 1700 nm using various fiber laser schemes and techniques.

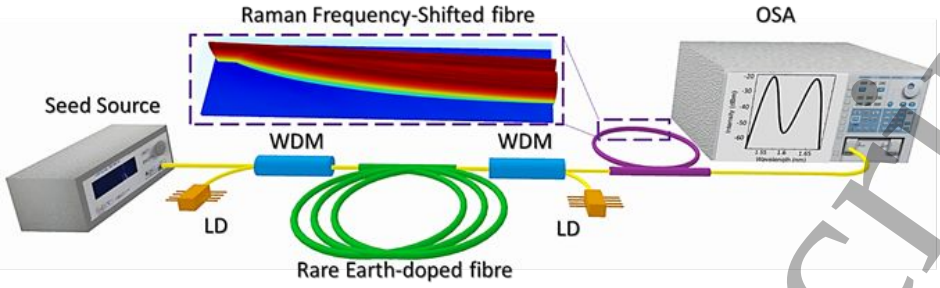


**Figure 5.** Setup of the SSFS-based fiber laser source and propagation of soliton in Raman self-frequency shifting fiber.

**Table 2.** Fiber laser systems emitting around 1700 nm.

| Technology | Pulse duration [fs] | Pulse energy, [nJ] | Ref. |
|---|---|---|---|
| FOPO | 450 | 40 | 171 |
| Bi-doped fiber MOPA | 630 | 5.7 | 177 |
| Tm-Ho | 630 | 0.02 | 181 |
| Er-doped & SSFS in SM telecom fiber | 384 | 0.03 | 203 |
| Er-doped & SSFS in DSF | 196 | 0.7 | 204 |
| Er-doped & SPM in DSF | 85 | 10.6 | 205 |
| Er-doped & SSFS in LMA | 75 | 9 | 206 |
| Er-doped & SSFS in LMA PCF | 100 | 10 | 207 |
| Er-doped & SSFS in PC rod | 70-80 | 50-65 | 208 |

Latest developments in 1700 nm laser sources pave the way for 3PEF imaging in the third biological window and, potentially, its future application to cancer detection in the digestive and urinary systems. However, to be competitive with standard clinical procedures (see Sections 1 and 2), an alternative methodology must meet some important requirements: high imaging speed, high label-free sensitivity/specificity, and deep tissue penetration.

Although no technique meets all needed criteria, their combination in a multimodal approach could overcome individual shortcomings and complement each other's information retrieved from the sample. In fact, nonlinear imaging methods can provide a high-resolution morphological characterisation of the examined tissues, while spectroscopic methods allow probing their composition and metabolic activity. Such an approach could improve tumour detection and margins identification. Nonetheless, one major challenge in the clinical application of multimodal imaging remains the adaptation of multiphoton techniques to an endoscopic environment.

## 6. Summary

Improving cancer detection, particularly in the digestive and urinary systems, constitutes a prominent objective for the future, especially in front of rising tumour incident rates and their associated costs. In order to evaluate the possibility of adding alternative tools to current clinical procedures, in this article we reviewed the relevant literature on the applications non-invasive optical methods (Raman, reflectance and autofluorescence, TPEF, SHG, THG, 3PEF, and CARS) to the study of gastrointestinal and urothelial tumours. Using these techniques, either in single modality or in a multimodal approach, many studies have already demonstrated the possibility to extract important morphochemical information from the label-free

examination of both *ex-vivo* and *in vivo* tissues. In fact, the analysis of spectra and images acquired from unstained bladder/gastric samples has proved the ability to highlight and quantify significant differences in metabolic activity and properties of normal and diseased tissues, such as molecular composition, oxygenation and morphological features. These parameters could be used for automated, fast, operator-independent evaluation of suspicious tissue areas or biopsies, providing a useful tool to complement white light imaging.

However, clinical implementations of photonics-based techniques for detecting gastrointestinal and bladder cancers require the use of endoscopes adapted to such task. Well-established solutions are already available for spectroscopic and imaging applications of linear optical techniques; instead, endoscopes for multiphoton imaging face many technological challenges and are still under development (although some have been successfully tested).

On the other hand, scattering and water absorption constitute major obstacles for single-photon techniques when examining deep tissue layers, which is of paramount importance for assessing tumour infiltration and could also help in verifying safe margins during its surgical removal. In this context, 2- and (even more) 3-photon excitation techniques provide clear advantages in tissue penetration, optical resolution and reduced photodamage. And while the majority of reviewed papers implemented SHG/TPEF microscopes, the latest developments in ultrafast laser sources – in particular, emitting around 1700 nm – could pave the way for increased use of THG and 3PEF imaging. The third biological window promises several advantages for working with deep tissues for multiphoton imaging. In this regard, Table 3 reports the advantages and disadvantages of all the techniques reviewed in this article.

**Table 3.** List of advantages and disadvantages of major photonics-based techniques.

| Technique | Advantages | Disadvantages |
|---|---|---|
| Autofluorescence | • Fast imaging<br>• Detection of intrinsic fluorophores*<br>• Allow spectroscopy analysis | • Low penetration depth<br>• Limited molecular characterisation |
| Reflectance | • Fast imaging<br>• Allow spectroscopy analysis<br>• Simple Setup | • Low penetration depth<br>• Limited molecular characterisation |
| Raman | • High-detailed molecular characterisation<br>• Medium penetration depth | • Long integration time |
| SHG | • High spatial resolution<br>• High penetration depth<br>• Provide structure information for non-centrosymmetric molecules | • Non molecular identity<br>• Directionality<br>• Need a ultrashort source |
| TPEF/3PEF | • High spatial resolution<br>• High penetration depth<br>• Detection of intrinsic fluorophores*<br>• Allow spectroscopy analysis | • Only few fluorophores can be excited*<br>• Limited molecular characterisation<br>• Requires ultrashort source |
| CARS | • High spatial resolution<br>• High penetration depth | • Limited molecular characterisation<br>• Directionality<br>• Requires two ultrashort sources<br>• Complex setup |
| THG | • High spatial resolution<br>• High penetration depth<br>• Provide structure information of interfaces and optical heterogeneities | • Non molecular identity<br>• Directionality<br>• Requires ultrashort source |

* The fluorophores that can be excited depend on the source spec (wavelength, broadband and time duration) available in the market.

Full exploitation of the possibilities offered by the photonics-based techniques summarized in this review requires correlating the performance of these techniques with an in-depth knowledge of the molecular and metabolic modifications connected with the observed spectroscopic and microscopic readouts. Suitable preclinical systems aimed at reconstructing the tumor microenvironment allow performing in-depth genetic and molecular analyses that are often impossible on clinical samples. These techniques include the growth of three-dimensional cultures of stabilized cell lines (spheroids)[220,221] with varying degrees

of aggressiveness and the production of organoids from clinical samples when sufficient bioptic material is available[222–224]. Some examples of the application of spectroscopic techniques on organoids and spheroids from tumors of the bladder and gastrointestinal tract have been published[225-232]. The integration of these spectroscopic analyses with molecular and post-genomic analyses will allow a more refined correlation of spectroscopic and biochemical properties, whose translation in the clinical setting may allow higher resolution patient staging, making it possible to design more effective and less toxic patient-specific personalized therapies[233,234].

The implementation of label-free photonics-based techniques in the clinical environment represents an ambitious solution for increasing the diagnostic efficacy of current gold standard tests based on WLI. While each technique has strengths and weaknesses, their combination in a multimodal approach could overcome the individual shortcomings and significantly improve cancer diagnosis. A recent example of such efforts is represented by the European Union Horizon 2020 project called AMPLITUDE (Advanced Multimodal Photonics Laser Imaging Tool for Urothelial Diagnosis in Endoscopy[14]), which aims to analyse spheroids and organoids derived from bladder tumours through Raman, TPEF and 3PEF imaging, and to develop a multimodal endoscope (combining all three techniques) specifically designed for urothelial cancer diagnosis. More in general, the literature reviewed in this article suggests that photonics may play an ever-increasing role in translational research and, particularly, in detecting tumours in the digestive and urinary systems.

## Acknowledgements

This project has received funding from the European Union's Horizon 2020 research and innovation programme under grant agreement No 871277 and is an initiative of the Photonics Public Private Partnership. G.C.O and P.L.A acknowledge funding form the Spanish Ministry of Economy and Competitiveness through the "Severo Ochoa" program for Centres of Excellence in R&D (CEX2019-000910-S), from Fundació Privada Cellex, Fundació Mir-Puig, Generalitat de Catalunya through the CERCA program and Laserlab-Europe EU-H2020 (871124). RG acknowledges Research Council of Finland (320165). G. C.-O., E. B. and D. S., contributed data analysis, manuscript preparation, writing and revising. A. K. and D. G. contributed to data analysis. All authors contributed to manuscript writing and revision. D. J., R. C., S. M., E. R., F. S. P., M. V., P. L.A., R.G contributed project conceptualization supervision and funding.

## Competing interests

The authors declare no competing interests.

## References

[1] Sung, H., Ferlay, J., Siegel, R.L., Laversanne, M., Soerjomataram, I., Jemal, A., and Bray, F., "Global Cancer Statistics 2020: GLOBOCAN Estimates of Incidence and Mortality Worldwide for 36 Cancers in 185 Countries," CA: A Cancer Journal for Clinicians 71(3), 209–249 (2021).

[2] Ferlay, J., Steliarova-Foucher, E., Lortet-Tieulent, J., Rosso, S., Coebergh, J.W.W., Comber, H., Forman, D., and Bray, F., "Cancer incidence and mortality patterns in Europe: Estimates for 40 countries in 2012," European Journal of Cancer 49(6), 1374–1403 (2013).

[3] Ferlay, J., and Laversanne, M., "Global Cancer Observatory: Cancer Tomorrow. Lyon, France: International Agency for Research on Cancer" (2020).

[4] Cumberbatch, M.G.K., Cox, A., Teare, D., and Catto, J.W.F., "Contemporary occupational carcinogen exposure and bladder cancer," JAMA Oncology (2015).

[5] Antoni, S., Ferlay, J., Soerjomataram, I., Znaor, A., Jemal, A., and Bray, F., "Bladder Cancer Incidence and Mortality: A Global Overview and Recent Trends," European Urology 71(1), 96–108 (2017).

[6] Araghi, M., Soerjomataram, I., Jenkins, M., Brierley, J., Morris, E., Bray, F., and Arnold, M., "Global trends in colorectal cancer mortality: projections to the year 2035," International Journal of Cancer 144(12), 2992–3000 (2019).

[7] Fernando, H., Thota, S.S., Burtt, G., Waterfall, N., and Husain, I., "Importance of red patches diagnosed in cystoscopy for haematuria and lower urinary tract symptoms," Postgraduate Medical Journal 83(975), 62–63 (2007).

[8] Beg, S., Wilson, A., and Ragunath, K., "The use of optical imaging techniques in the gastrointestinal tract," Frontline Gastroenterology 7(3), 207–215 (2016).

[9] Oka, K., Iwai, N., Okuda, T., Hara, T., Inada, Y., Tsuji, T., Komaki, T., Sakagami, J., Naito, Y., et al., "Clinical Features of False-Negative Early Gastric Cancers: A Retrospective Study of Endoscopic Submucosal Dissection Cases," Gastroenterology Research and Practice 2021, 1–9 (2021).

[10] Fukuhara, H., Yamamoto, S., Karashima, T., and Inoue, K., "Photodynamic diagnosis and therapy for urothelial carcinoma and prostate cancer: new imaging technology and therapy," International Journal of Clinical Oncology 26(1), 18–25 (2021).

[11] Wu, J., Wang, Y.-C., Dai, B., Ye, D.-W., and Zhu, Y.-P., "Optical biopsy of bladder cancer using confocal laser endomicroscopy," International Urology and Nephrology 51(9), 1473–1479 (2019).

[12] Baria, E., Morselli, S., Anand, S., Fantechi, R., Nesi, G., Gacci, M., Carini, M., Serni, S., Cicchi, R., et al., "Label-free grading and staging of urothelial carcinoma through multimodal fibre-probe spectroscopy," Journal of Biophotonics 12(11), (2019).

[13] Morselli, S., Baria, E., Cicchi, R., Liaci, A., Sebastianelli, A., Nesi, G., Serni, S., Pavone, F.S., and Gacci, M., "The feasibility of multimodal fiber optic spectroscopy analysis in bladder cancer detection, grading, and staging," Urologia Journal 88(4), 306–314 (2021).

[14] Kurilchik, S., Gacci, M., Cicchi, R., Pavone, F.S., Morselli, S., Serni, S., Chou, M.H., Närhi, M., Rafailov, E., et al., "Advanced multimodal laser imaging tool for urothelial carcinoma diagnosis (AMPLITUDE)," JPhys Photonics 2(2), (2020).

[15] Castro-Olvera, G., Serni, S., Liaci, A., Morselli, S., Gacci, M., Nicoletti, R., and Loza-Alvarez, P., "Multimodal SWIR Laser Imaging for Assessment and Detection of Urothelial Carcinomas", in "Short-Wavelength Infrared Windows for Biomedical Applications", L. A. Sordillo and P. P. Sordillo, Eds., SPIE (2021).

[16] Yamamoto, S., Fukuhara, H., Karashima, T., and Inoue, K., "Real-world experience with 5-aminolevulinic acid for the photodynamic diagnosis of bladder cancer: Diagnostic accuracy and safety," Photodiagnosis and Photodynamic Therapy 32, 101999 (2020).

[17] Zheng, C., Lv, Y., Zhong, Q., Wang, R., and Jiang, Q., "Narrow band imaging diagnosis of bladder cancer: Systematic review and meta-analysis," BJU International (2012).

[18] Loidl, W., Schmidbauer, J., Susani, M., and Marberger, M., "Flexible Cystoscopy Assisted by Hexaminolevulinate Induced Fluorescence: A New Approach for Bladder Cancer Detection and Surveillance?," European Urology 47(3), 323–326 (2005).

[19] Bryan, R.T., Billingham, L.J., and Wallace, D.M.A., "Narrow-band imaging flexible cystoscopy in the detection of recurrent urothelial cancer of the bladder," BJU International 101(6), 702–706 (2008).

[20] Kamphuis, G.M., de Bruin, D.M., Brandt, M.J., Knoll, T., Conort, P., Lapini, A., Dominguez-Escrig, J.L., and de la Rosette, J.J.M.C.H., "Comparing Image Perception of Bladder Tumors in Four Different Storz Professional Image Enhancement System Modalities Using the íSPIES App," Journal of Endourology 30(5), 602–608 (2016).

[21] Marti, A., Lange, N., Van Den Bergh, H., Sedmera, D., Jichlinski, P., and Kucera, P., "Optimisation of the formation and distribution of protoporphyrin IX in the urothelium: an in vitro approach," Journal of Urology 162(2), 546–552 (1999).

[22] Holtl, L., Eder, I.E., Klocker, H., Hobisch, A., Bartsch, G., and Stenzl, A., "Photodynamic Diagnosis with 5-Aminolevulinic Acid in the Treatment of Secondary Urethral Tumors: First in vitro and in vivo Results," European Urology 39(2), 178–182 (2001).

[23] Chauhan, S.S., Abu Dayyeh, B.K., Bhat, Y.M., Gottlieb, K.T., Hwang, J.H., Komanduri, S., Konda, V., Lo, S.K., Manfredi, M.A., et al., "Confocal laser endomicroscopy," Gastrointestinal Endoscopy 80(6), 928–938 (2014).

[24] Neumann, H., Kiesslich, R., Wallace, M.B., and Neurath, M.F., "Confocal Laser Endomicroscopy: Technical Advances and Clinical Applications," Gastroenterology 139(2), 388-392.e2 (2010).

[25] Marien, A., Rock, A., Maadarani, K.E., Francois, C., Gosset, P., Mauroy, B., and Bonnal, J.-L., "Urothelial Tumors and Dual-Band Imaging: A New Concept in Confocal Laser Endomicroscopy," Journal of Endourology 31(5), 538–544 (2017).

[26] Wiesner, C., Jäger, W., Salzer, A., Biesterfeld, S., Kiesslich, R., Hampel, C., Thüroff, J.W., and Goetz, M., "Confocal laser endomicroscopy for the diagnosis of urothelial bladder neoplasia: a technology of the future?," BJU International 107(3), 399–403 (2011).

[27] Bui, D., Mach, K.E., Zlatev, D.V., Rouse, R.V., Leppert, J.T., and Liao, J.C., "A Pilot Study of In Vivo Confocal Laser Endomicroscopy of Upper Tract Urothelial Carcinoma," Journal of Endourology 29(12), 1418–1423 (2015).

[28] Beji, S., Wrist Lam, G., Østergren, P.B., Toxvaerd, A., Sønksen, J., and Fode, M., "Diagnostic value of probe-based confocal laser endomicroscopy versus conventional endoscopic biopsies of non-muscle invasive bladder tumors: a pilot study," Scandinavian Journal of Urology 55(1), 36–40 (2021).

[29] Fugazza, A., Gaiani, F., Carra, M.C., Brunetti, F., Lévy, M., Sobhani, I., Azoulay, D., Catena, F., de'Angelis, G.L., et al., "Confocal Laser Endomicroscopy in Gastrointestinal and Pancreatobiliary Diseases: A Systematic Review and Meta-Analysis," BioMed Research International 2016, 1–31 (2016).

[30] Zonios, G., Bykowski, J., and Kollias, N., "Skin Melanin, Hemoglobin, and Light Scattering Properties can be Quantitatively Assessed In Vivo Using Diffuse Reflectance Spectroscopy," Journal of Investigative Dermatology 117(6), 1452–1457 (2001).

[31] Filip, M., "Autofluorescence imaging and magnification endoscopy," World Journal of Gastroenterology 17(1), 9 (2011).

[32] Wong Kee Song, L.-M., Banerjee, S., Desilets, D., Diehl, D.L., Farraye, F.A., Kaul, V., Kethu, S.R., Kwon, R.S., Mamula, P., et al., "Autofluorescence imaging," Gastrointestinal Endoscopy 73(4), 647–650 (2011).

[33] Aihara, H., Tajiri, H., and Suzuki, T., "Application of Autofluorescence Endoscopy for Colorectal Cancer Screening: Rationale and an Update," Gastroenterology Research and Practice 2012, 1–5 (2012).

[34] Tajiri, H., "Autofluorescence endoscopy for the gastrointestinal tract," Proceedings of the Japan Academy. Series B, Physical and Biological Sciences 83(8), 248–255 (2007).

[35] Lakowicz, J.R., "Principles of Fluorescence Spectroscopy, 3rd edition" (2006).

[36] Wagnieres, G.A., Star, W.M., and Wilson, B.C., "In vivo Fluorescence Spectroscopy and Imaging for Oncological Applications," Photochemistry and Photobiology 68(5), 603–632 (1998).

[37] Croce, A.C., and Bottiroli, G., "Autofluorescence spectroscopy and imaging: a tool for biomedical research and diagnosis," European Journal of Histochemistry 58(2461), 320–337 (2014).[38] Bachmann, L., Zezell, D.M., Ribeiro, A. da C., Gomes, L., and Ito, A.S., "Fluorescence Spectroscopy of Biological Tissues—A Review," Applied Spectroscopy Reviews 41(6), 575–590 (2006).

[39] Moriichi, K., Fujiya, M., and Okumura, T., "The efficacy of autofluorescence imaging in the diagnosis of colorectal diseases," Clinical Journal of Gastroenterology 9(4), 175–183 (2016).

[40] Movasaghi, Z., Rehman, S., and Rehman, I.U., "Raman Spectroscopy of Biological Tissues," Applied Spectroscopy Reviews 42(5), 493–541 (2007).

[41] Choo-Smith, L.-P., Edwards, H.G.M., Endtz, H.P., Kros, J.M., Heule, F., Barr, H., Robinson, J.S., Bruining, H.A., and Puppels, G.J., "Medical applications of Raman spectroscopy: From proof of principle to clinical implementation," Biopolymers 67(1), 1–9 (2002).

[42] Alizadeh, M., Merino, D., Lombardo, G., Lombardo, M., Mencucci, R., Ghotbi, M., and Loza-Alvarez, P., "Identifying crossing collagen fibers in human corneal tissues using pSHG images," Biomedical Optics Express 10(8), 3875 (2019).

[43] Chen, W.-C., Chen, Y.-J., Lin, S.-T., Hung, W.-H., Chan, M.-C., Wu, I.-C., Wu, M.-T., Kuo, C.-T., Das, S., et al., "Label-free characterization of collagen fibers in cancerous esophagus tissues using ratiometric nonlinear optical microscopy," Experimental Biology and Medicine 245(14), 1213–1221 (2020).

[44] Lombardo, M., Merino, D., Loza-Alvarez, P., and Lombardo, G., "Translational label-free nonlinear imaging biomarkers to classify the human corneal microstructure," Biomedical Optics Express 6(8), 2803 (2015).

[45] Psilodimitrakopoulos, S., Artigas, D., Soria, G., Amat-Roldan, I., Planas, A.M., and Loza-Alvarez, P., "Quantitative discrimination between endogenous SHG sources in mammalian tissue, based on their polarization response," Optics Express 17(12), 10168 (2009).

[46] Psilodimitrakopoulos, S., Petegnief, V., Soria, G., Amat-Roldan, I., Artigas, D., Planas, A.M., and Loza-Alvarez, P., "Estimation of the effective orientation of the SHG source in primary cortical neurons," Optics Express 17(16), 14418 (2009).

[47] Psilodimitrakopoulos, S., Loza-Alvarez, P., and Artigas, D., "Fast monitoring of in-vivo conformational changes in myosin using single scan polarization-SHG microscopy," Biomedical Optics Express 5(12), 4362 (2014).

[48] Amat-Roldan, I., Psilodimitrakopoulos, S., Loza-Alvarez, P., and Artigas, D., "Fast image analysis in polarization SHG microscopy," Optics Express 18(16), 17209 (2010).

[49] Psilodimitrakopoulos, S., Amat-Roldan, I., Loza-Alvarez, P., and Artigas, D., "Effect of molecular organization on the image histograms of polarization SHG microscopy," Biomedical Optics Express 3(10), 2681 (2012).

[50] Aviles-Espinosa, R., "Third-harmonic generation for the study of 'Caenorhabditis elegans' embryogenesis," Journal of Biomedical Optics 15(4), 046020 (2010).

[51] Klinger, A., Krapf, L., Orzekowsky-Schroeder, R., Koop, N., Vogel, A., and Hüttmann, G., "Intravital autofluorescence 2-photon microscopy of murine intestinal mucosa with ultra-broadband femtosecond laser pulse excitation: image quality, photodamage, and inflammation," Journal of Biomedical Optics 20(11), 1 (2015).

[52] Chaumel, J., Marsal, M., Gómez-Sánchez, A., Blumer, M., Gualda, E.J., de Juan, A., Loza-Alvarez, P., and Dean, M.N., "Autofluorescence of stingray skeletal cartilage: hyperspectral imaging as a tool for histological characterization," Discover Materials 1(1), 16 (2021).

[53] Oheim, M., Beaurepaire, E., Chaigneau, E., Mertz, J., and Charpak, S., "Two-photon microscopy in brain tissue: parameters influencing the imaging depth," Journal of Neuroscience Methods 111(1), 29–37 (2001).

[54] Resan, B., Aviles-Espinosa, R., Kurmulis, S., Licea-Rodriguez, J., Brunner, F., Rohrbacher, A., Artigas, D., Loza-Alvarez, P., and Weingarten, K.J., "Two-photon fluorescence imaging with 30 fs laser system tunable around 1 micron," Optics Express 22, 16456–16461 (2014).

[55] De Meulenaere, E., Chen, W.-Q., Van Cleuvenbergen, S., Zheng, M.-L., Psilodimitrakopoulos, S., Paesen, R., Taymans, J.-M., Ameloot, M., Vanderleyden, J., et al., "Molecular engineering of chromophores for combined second-harmonic and two-photon fluorescence in cellular imaging," Chemical Science 3(4), 984 (2012).

[56] Aviles-Espinosa, R., Filippidis, G., Hamilton, C., Malcolm, G., Weingarten, K.J., Südmeyer, T., Barbarin, Y., Keller, U., Santos, S.I.C.O., et al., "Compact ultrafast semiconductor disk laser: targeting GFP based nonlinear applications in living organisms," Biomedical Optics Express 2(4), 739 (2011).

[57] Wang, T., and Xu, C., "Three-photon neuronal imaging in deep mouse brain," Optica 7(8), 947–960 (2020).

[58] Streich, L., Boffi, J.C., Wang, L., Alhalaseh, K., Barbieri, M., Rehm, R., Deivasigamani, S., Gross, C.T., Agarwal, A., and Prevedel, R., "High-resolution structural and functional deep brain imaging using adaptive optics three-photon microscopy," Nature Methods 18, 1253–1258 (2021).

[59] Kapadia, C.R., Cutruzzola, F.W., O'Brien, K.M., Stetz, M.L., Enriquez, R., and Deckelbaum, L.I., "Laser-induced fluorescence spectroscopy of human colonic mucosa," Gastroenterology 99(1), 150–157 (1990).

[60] Marchesini, R., Brambilla, M., Pignoli, E., Bottiroli, G., Croce, A.C., Dal Fante, M., Spinelli, P., and di Palma, S., "Light-induced fluorescence spectroscopy of adenomas, adenocarcinomas and non-neoplastic mucosa in human colon I. In vitro measurements," Journal of Photochemistry and Photobiology B: Biology 14(3), 219–230 (1992).

[61] Chwirot, B.W., Chwirot, S., Jedrzejczyk, W., Jackowski, M., Raczyńska, A.M., Winczakiewicz, J., and Dobber, J., "Ultraviolet laser-induced fluorescence of human stomach tissues: Detection of cancer tissues by imaging techniques," Lasers in Surgery and Medicine 21(2), 149–158 (1997).

[62] Cothren, R.M., Richards-Kortum, R., Sivak, M.V., Fitzmaurice, M., Rava, R.P., Boyce, G.A., Doxtader, M., Blackman, R., Ivanc, T.B., et al., "Gastrointestinal tissue diagnosis by laser-induced fluorescence spectroscopy at endoscopy," Gastrointestinal Endoscopy 36(2), 105–111 (1990).

[63] Ge, Z., Schomacker, K.T., and Nishioka, N.S., "Identification of Colonic Dysplasia and Neoplasia by Diffuse Reflectance Spectroscopy and Pattern Recognition Techniques" 52, 833–839 (1998).

[64] Mourant, J.R., "Elastic scattering spectroscopy as a diagnostic tool for differentiating pathologies in the gastrointestinal tract: preliminary testing," Journal of Biomedical Optics 1(2), 192 (1996).

[65] Stone, N., Kendall, C., Shepherd, N., Crow, P., and Barr, H., "Near-infrared Raman spectroscopy for the classification of epithelial pre-cancers and cancers," Journal of Raman Spectroscopy 33(7), 564–573 (2002).

[66] Kendall, C., Stone, N., Shepherd, N., Geboes, K., Warren, B., Bennett, R., and Barr, H., "Raman spectroscopy, a potential tool for the objective identification and classification of neoplasia in Barrett's oesophagus," The Journal of Pathology 200(5), 602–609 (2003).

[67] Teh, S.K., Zheng, W., Ho, K.Y., Teh, M., Yeoh, K.G., and Huang, Z., "Diagnosis of gastric cancer using near-infrared Raman spectroscopy and classification and regression tree techniques," Journal of Biomedical Optics 13(3), 034013 (2008).

[68] Kobayashi, M., Tajiri, H., Seike, E., Shitaya, M., Tounou, S., Mine, M., and Oba, K., "Detection of early gastric cancer by a real-time autofluorescence imaging system," Cancer Letters 165(2), 155–159 (2001).

[69] Mayinger, B., Horner, P., Jordan, M., Gerlach, C., Horbach, T., Hohenberger, W., and Hahn, E.G., "Light-induced autofluorescence spectroscopy for the endoscopic detection of esophageal cancer," Gastrointestinal Endoscopy 54(2), 195–201 (2001).

[70] Xiao, S.D., Ge, Z.Z., Zhong, L., and Luo, H.Y., "Diagnosis of gastric cancer by using autofluorescence spectroscopy," Chinese Journal of Digestive Diseases 3(3), 99–102 (2002).

[71] Mayinger, B., Jordan, M., Horbach, T., Horner, P., Gerlach, C., Mueller, S., Hohenberger, W., and Hahn, E.G., "Evaluation of in vivo endoscopic autofluorescence spectroscopy in gastric cancer," Gastrointestinal Endoscopy 59(2), 191–198 (2004).

[72] Kamath, S.D., D'souza, C.S., Mathew, S., George, S.D., Santhosh, C., and Mahato, K.K., "A pilot study on colonic mucosal tissues by fluorescence spectroscopy technique: Discrimination by principal component analysis (PCA) and artificial neural network (ANN) analysis," Journal of Chemometrics 22(6), 408–416 (2008).

[73] Bergholt, M.S., Zheng, W., Lin, K., Ho, K.Y., Teh, M., Yeoh, K.G., So, J.B.Y., and Huang, Z., "Combining near-infrared-excited autofluorescence and Raman spectroscopy improves in vivo diagnosis of gastric cancer," Biosensors and Bioelectronics 26(10), 4104–4110 (2011).

[74] Boerwinkel, D.F., Holz, J.A., Hawkins, D.M., Curvers, W.L., Aalders, M.C., Weusten, B.L., Visser, M., Meijer, S.L., and Bergman, J.J., "Fluorescence spectroscopy incorporated in an Optical Biopsy System for the detection of early neoplasia in Barrett's esophagus: Optical Biopsy System," Diseases of the Esophagus 28(4), 345–351 (2015).

[75] Ehlen, L., Zabarylo, U.J., Speichinger, F., Bogomolov, A., Belikova, V., Bibikova, O., Artyushenko, V., Minet, O., Beyer, K., et al., "Synergy of Fluorescence and Near-Infrared Spectroscopy in Detection of Colorectal Cancer," Journal of Surgical Research 242, 349–356 (2019).

[76] Dhar, A., Johnson, K.S., Novelli, M.R., Bown, S.G., Bigio, I.J., Lovat, L.B., and Bloom, S.L., "Elastic scattering spectroscopy for the diagnosis of colonic lesions: initial results of a novel optical biopsy technique," Gastrointestinal Endoscopy 63(2), 257–261 (2006).

[77] Akbari, H., Uto, K., Kosugi, Y., Kojima, K., and Tanaka, N., "Cancer detection using infrared hyperspectral imaging," Cancer Science 102(4), 852–857 (2011).

[78] Kiyotoki, S., Nishikawa, J., Okamoto, T., Hamabe, K., Saito, M., Goto, A., Fujita, Y., Hamamoto, Y., Takeuchi, Y., et al., "New method for detection of gastric cancer by hyperspectral imaging: a pilot study," Journal of Biomedical Optics 18(2), 026010 (2013).

[79] Evers, D.J., Nachabé, R., Hompes, D., van Coevorden, F., Lucassen, G.W., Hendriks, B.H.W., van Velthuysen, M.-L.F., Wesseling, J., and Ruers, T.J.M., "Optical sensing for tumor detection in the liver," European Journal of Surgical Oncology (EJSO) 39(1), 68–75 (2013).

[80] Kumashiro, R., Konishi, K., Chiba, T., Akahoshi, T., Nakamura, S., Murata, M., Tomikawa, M., Matsumoto, T., Maehara, Y., et al., "Integrated Endoscopic System Based on Optical Imaging and Hyperspectral Data Analysis for Colorectal Cancer Detection," Anticancer Research 36(8), 3925 (2016).

[81] Han, Z., Zhang, A., Wang, X., Sun, Z., Wang, M.D., and Xie, T., "In vivo use of hyperspectral imaging to develop a noncontact endoscopic diagnosis support system for malignant colorectal tumors," Journal of Biomedical Optics 21(1), 016001 (2016).

[82] Tanis, E., Evers, D.J., Spliethoff, J.W., Pully, V.V., Kuhlmann, K., van Coevorden, F., Hendriks, B.H.W., Sanders, J., Prevoo, W., et al., "In vivo tumor identification of colorectal liver metastases with diffuse reflectance and fluorescence spectroscopy," Lasers in Surgery and Medicine 48(9), 820–827 (2016).

[83] Keller, A., Bialecki, P., Wilhelm, T.J., and Vetter, M.K., "Diffuse reflectance spectroscopy of human liver tumor specimens - towards a tissue differentiating optical biopsy needle using light emitting diodes," Biomedical Optics Express 9(3), 1069 (2018).

[84] Baltussen, E.J.M., Brouwer de Koning, S.G., Sanders, J., Aalbers, A.G.J., Kok, N.F.M., Beets, G.L., Hendriks, B.H.W., Sterenborg, H.J.C.M., Kuhlmann, K.F.D., et al., "Tissue diagnosis during colorectal cancer surgery using optical sensing: an in vivo study," Journal of Translational Medicine 17(1), 333 (2019).

[85] Nogueira, M.S., Maryam, S., Amissah, M., Lu, H., Lynch, N., Killeen, S., O'Riordain, M., and Andersson-Engels, S., "Evaluation of wavelength ranges and tissue depth probed by diffuse reflectance spectroscopy for colorectal cancer detection," Scientific Reports 11(1), 798 (2021).

[86] Huang, Z., Teh, S.K., Zheng, W., Lin, K., Ho, K.Y., Teh, M., and Yeoh, K.G., "In vivo detection of epithelial neoplasia in the stomach using image-guided Raman endoscopy," Biosensors and Bioelectronics 26(2), 383–389 (2010).

[87] Teh, S.K., Zheng, W., Ho, K.Y., Teh, M., Yeoh, K.G., and Huang, Z., "Near-infrared Raman spectroscopy for early diagnosis and typing of adenocarcinoma in the stomach," British Journal of Surgery 97(4), 550–557 (2010).

[88] Bergholt, M.S., Zheng, W., Lin, K., Ho, K.Y., Teh, M., Yeoh, K.G., Yan So, J.B., and Huang, Z., "In vivo diagnosis of gastric cancer using Raman endoscopy and ant colony optimization techniques," International Journal of Cancer 128(11), 2673–2680 (2011).

[89] Kawabata, T., Kikuchi, H., Okazaki, S., Yamamoto, M., Hiramatsu, Y., Yang, J., Baba, M., Ohta, M., Kamiya, K., et al., "Near-Infrared Multichannel Raman Spectroscopy with a 1064 nm Excitation Wavelength for Ex Vivo Diagnosis of Gastric Cancer," Journal of Surgical Research 169(2), e137–e143 (2011).

[90] Duraipandian, S., "Real-time Raman spectroscopy for in vivo, online gastric cancer diagnosis during clinical endoscopic examination," Journal of Biomedical Optics 17(8), 081418 (2012).

[91] Bergholt, M.S., Zheng, W., Ho, K.Y., Teh, M., Yeoh, K.G., So, J.B.Y., Shabbir, A., and Huang, Z., "Fiber-optic Raman spectroscopy probes gastric carcinogenesis in vivo at endoscopy," Journal of Biophotonics 6(1), 49–59 (2013).

[92] Jin, S., and Mao, H., "Near-infrared Raman spectroscopy for diagnosis of gastric cancer" 34(3), 391–5 (2014).

[93] Wang, J., Lin, K., Zheng, W., Ho, K.Y., Teh, M., Yeoh, K.G., and Huang, Z., "Fiber-optic Raman spectroscopy for in vivo diagnosis of gastric dysplasia," Faraday Discussions 187, 377–392 (2016).

[94] Petersen, D., Naveed, P., Ragheb, A., Niedieker, D., El-Mashtoly, S.F., Brechmann, T., Kötting, C., Schmiegel, W.H., Freier, E., et al., "Raman fiber-optical method for colon cancer detection: Cross-validation and outlier identification approach," Spectrochimica Acta Part A: Molecular and Biomolecular Spectroscopy 181, 270–275 (2017).

[95] Ell, C., "Improving endoscopic resolution and sampling: fluorescence techniques," Gut 52(90004), 30iv–3033 (2003).

[96] Angelova, L., Borisova, E., Zhelyazkova, Al., Keremedchiev, M., Vladimirov, B., and Avramov, L., "Fluorescence spectroscopy of gastrointestinal tumors: in vitro studies and in vivo clinical applications," presented at 1st International Conference "Biophotonics Riga 2013," 18 November 2013, Riga, Latvia, 903209.

[97] Liu, L., Lin, L., Li, W., Yang, C., Huang, Z., Xie, S., and Li, B., "Characterizing autofluorescence generated from endogenous porphyrins in cancerous tissue of human colon: case studies," presented at SPIE BiOS, 19 March 2013, San Francisco, California, USA, 857703.

[98] Teh, S.K., Zheng, W., Ho, K.Y., Teh, M., Yeoh, K.G., and Huang, Z., "Diagnostic potential of near-infrared Raman spectroscopy in the stomach: differentiating dysplasia from normal tissue," British Journal of Cancer 98(2), 457–465 (2008).

[99] Zheng, W., Li, D., Li, S., Zeng, Y., Yang, Y., and Qu, J.Y., "Diagnostic value of nonlinear optical signals from collagen matrix in the detection of epithelial precancer," Optics Letters 36(18), 3620 (2011).

[100] Orzekowsky-Schroeder, R., Klinger, A., Martensen, B., Blessenohl, M., Gebert, A., Vogel, A., and Hüttmann, G., "In vivo spectral imaging of different cell types in the small intestine by two-photon excited autofluorescence," Journal of Biomedical Optics 16(11), 116025 (2011).

[101] Cicchi, R., Sturiale, A., Nesi, G., Kapsokalyvas, D., Alemanno, G., Tonelli, F., and Pavone, F.S., "Multiphoton morpho-functional imaging of healthy colon mucosa, adenomatous polyp and adenocarcinoma," Biomedical Optics Express 4(7), 1204 (2013).

[102] Makino, T., Jain, M., Montrose, D.C., Aggarwal, A., Sterling, J., Bosworth, B.P., Milsom, J.W., Robinson, B.D., Shevchuk, M.M., et al., "Multiphoton Tomographic Imaging: A Potential Optical Biopsy Tool for Detecting Gastrointestinal Inflammation and Neoplasia," Cancer Prevention Research 5(11), 1280–1290 (2012).

[103] Chen, J., Wong, S., Nathanson, M.H., Chen, J., and Jain, D., "Evaluation of Barrett Esophagus by Multiphoton Microscopy," Archives of Pathology & Laboratory Medicine 138(2), 204–212 (2014).

[104] Stanciu, S.G., Xu, S., Peng, Q., Yan, J., Stanciu, G.A., Welsch, R.E., So, P.T.C., Csucs, G., and Yu, H., "Experimenting Liver Fibrosis Diagnostic by Two Photon Excitation Microscopy and Bag-of-Features Image Classification," Scientific Reports 4(1), 4636 (2015).

[105] Li, L., Jiang, W., Yang, Y., Chen, Z., Feng, C., Li, H., Guan, G., and Chen, J., "Identification of dirty necrosis in colorectal carcinoma based on multiphoton microscopy," Journal of Biomedical Optics 19(6), 066008 (2014).

[106] Schueth, A., van Zandvoort, M.A.M.J., Buurman, W.A., and van Koeveringe, G.A., "Murine Bladder Imaging by 2-Photon Microscopy: An Experimental Study of Morphology," Journal of Urology 192(3), 973–980 (2014).

[107] Yan, J., Zhuo, S., Chen, G., Milsom, J.W., Zhang, H., Lu, J., Zhu, W., Xie, S., Chen, J., et al., "Real-time optical diagnosis for surgical margin in low rectal cancer using multiphoton microscopy," Surgical Endoscopy 28(1), 36–41 (2014).

[108] Zhou, Y., Kang, D., Yang, Z., Li, L., Zhuo, S., Zhu, X., Zhou, Y., and Chen, J., "Imaging normal and cancerous human gastric muscular layer in transverse and longitudinal sections by multiphoton microscopy: Imaging the human gastric muscular layer by using MPM," Scanning 38(4), 357–364 (2016).

[109] Skala, M.C., Squirrell, J.M., Vrotsos, K.M., Eickhoff, J.C., Gendron-Fitzpatrick, A., Eliceiri, K.W., and Ramanujam, N., "Multiphoton Microscopy of Endogenous Fluorescence Differentiates Normal, Precancerous, and Cancerous Squamous Epithelial Tissues," Cancer Research 65(4), 1180–1186 (2005).

[110] Matsui, T., Mizuno, H., Sudo, T., Kikuta, J., Haraguchi, N., Ikeda, J., Mizushima, T., Yamamoto, H., Morii, E., et al., "Non-labeling multiphoton excitation microscopy as a novel diagnostic tool for discriminating normal tissue and colorectal cancer lesions," Scientific Reports 7(1), 6959 (2017).

[111] Sarri, B., Canonge, R., Audier, X., Simon, E., Wojak, J., Caillol, F., Cador, C., Marguet, D., Poizat, F., et al., "Fast stimulated Raman and second harmonic generation imaging for intraoperative gastro-intestinal cancer detection," Scientific Reports 9(1), 10052 (2019).

[112] Li, L., Kang, D., Huang, Z., Zhan, Z., Feng, C., Zhou, Y., Tu, H., Zhuo, S., and Chen, J., "Multimodal multiphoton imaging for label-free monitoring of early gastric cancer," BMC Cancer 19(1), 295 (2019).

[113] Shen, B., Yan, J., Wang, S., Zhou, F., Zhao, Y., Hu, R., Qu, J., and Liu, L., "Label-free whole-colony imaging and metabolic analysis of metastatic pancreatic cancer by an autoregulating flexible optical system," Theranostics 10(4), 1849–1860 (2020).

[114] Zhang, H., Chen, Y., Cao, D., Li, W., Jing, Y., Zhong, H., Liu, H., and Zhu, X., "Optical biopsy of laryngeal lesions using femtosecond multiphoton microscopy," Biomedical Optics Express 12(3), 1308 (2021).

[115] D'Hallewin, M.A., Baert, L., and Vanherzeele, H., "In Vivo Fluorescence Detection of Human Bladder Carcinoma Without Sensitizing Agents," The Journal of The American Paraplegia Society 17(4), 161–164 (1994).

[116] Koenig, F., McGovern, F.J., Althausen, A.F., Deutsch, T.F., and Schomacker, K.T., "Laser Induced Autofluorescence Diagnosis of Bladder Cancer," Journal of Urology 156(5), 1597–1601 (1996).

[117] Zaak, D., Stepp, H., Baumgartner, R., Schneede, P., Waidelich, R., Frimberger, D., Hartmann, A., Knchel, R., Hofstetter, A., et al., "Ultraviolet-excited (308 nm) autofluorescence for bladder cancer detection," Urology 60(6), 1029–1033 (2002).

[118] Aboumarzouk, O., Valentine, R., Buist, R., Ahmad, S., Nabi, G., Eljamel, S., Moseley, H., and Kata, S.G., "Laser-induced autofluorescence spectroscopy: Can it be of importance in detection of bladder lesions?," Photodiagnosis and Photodynamic Therapy 12(1), 76–83 (2015).

[119] Kriegmair, M.C., Honeck, P., Theuring, M., Bolenz, C., and Ritter, M., "Wide-field autofluorescence-guided TUR-B for the detection of bladder cancer: a pilot study," World Journal of Urology 36(5), 745–751 (2018).

[120] Anidjar, M., "Ultraviolet laser-induced autofluorescence distinction between malignant and normal urothelial cells and tissues," Journal of Biomedical Optics 1(3), 335 (1996).

[121] Zheng, W., Lau, W., Cheng, C., Soo, K.C., and Olivo, M., "Optimal excitation-emission wavelengths for autofluorescence diagnosis of bladder tumors," International Journal of Cancer 104(4), 477–481 (2003).

[122] Mourant, J.R., Bigio, I.J., Boyer, J., Conn, R.L., Johnson, T., and Shimada, T., "Spectroscopic diagnosis of bladder cancer with elastic light scattering," Lasers in Surgery and Medicine 17(4), 350–357 (1995).

[123] Koenig, F., Larne, R., Enquist, H., McGovern, F.J., Schomacker, K.T., Kollias, N., and Deutsch, T.F., "Spectroscopic measurement of diffuse reflectance for enhanced detection of bladder carcinoma," Urology 51(2), 342–345 (1998).

[124] Slaton, J., Hurst, R., Davis, C., Rajaputra, P., You, Y., Bartels, K., and Piao, D., "MP61-09 Early Development of Intravesical Reflectance Spectroscopy for Bladder Tumor Detection and Staging," Journal of Urology 195(4S), (2016).

[125] Rosenzweig, B., Herr, H., and Coleman, J.A., [Narrow Band Imaging in the Evaluation of Upper Tract Urothelial Cancer] , in Urothelial Malignancies of the Upper Urinary Tract, M. Eshghi, Ed., Springer International Publishing, Cham, 129–143 (2018).

[126] Herr, H.W., and Donat, S.M., "A comparison of white-light cystoscopy and narrow-band imaging cystoscopy to detect bladder tumour recurrences," BJU International 102(9), 1111–1114 (2008).

[127] Tatsugami, K., Kuroiwa, K., Kamoto, T., Nishiyama, H., Watanabe, J., Ishikawa, S., Shinohara, N., Sazawa, A., Fukushima, S., et al., "Evaluation of Narrow-Band Imaging as a Complementary Method for the Detection of Bladder Cancer," Journal of Endourology 24(11), 1807–1811 (2010).

[128] Chen, G., Wang, B., Li, H., Ma, X., Shi, T., and Zhang, X., "Applying narrow-band imaging in complement with white-light imaging cystoscopy in the detection of urothelial carcinoma of the bladder," Urologic Oncology: Seminars and Original Investigations 31(4), 475–479 (2013).

[129] Ye, Z., Hu, J., Song, X., Li, F., Zhao, X., Chen, S., Wang, X., He, D., Fan, J., et al., "A comparison of NBI and WLI cystoscopy in detecting non-muscle-invasive bladder cancer: A prospective, randomized and multi-center study," Scientific Reports 5(1), 10905 (2015).

[130] Crow, P., Uff, J.S., Farmer, J.A., Wright, M.P., and Stone, N., "The use of Raman spectroscopy to identify and characterize transitional cell carcinoma in vitro," BJU International 93(9), 1232–1236 (2004).

[131] Crow, P., Molckovsky, A., Stone, N., Uff, J., Wilson, B., and WongKeeSong, L.-M., "Assessment of fiberoptic near-infrared raman spectroscopy for diagnosis of bladder and prostate cancer," Urology 65(6), 1126–1130 (2005).

[132] Draga, R.O.P., Grimbergen, M.C.M., Vijverberg, P.L.M., Swol, C.F.P. van, Jonges, T.G.N., Kummer, J.A., and Ruud Bosch, J.L.H., "In Vivo Bladder Cancer Diagnosis by High-Volume Raman Spectroscopy," Analytical Chemistry 82(14), 5993–5999 (2010).

[133] Barman, I., Dingari, N.C., Singh, G.P., Kumar, R., Lang, S., and Nabi, G., "Selective sampling using confocal Raman spectroscopy provides enhanced specificity for urinary bladder cancer diagnosis," Analytical and Bioanalytical Chemistry 404(10), 3091–3099 (2012).

[134] Cordero, E., Rüger, J., Marti, D., Mondol, A.S., Hasselager, T., Mogensen, K., Hermann, G.G., Popp, J., and Schie, I.W., "Bladder tissue characterization using probe-based Raman spectroscopy: Evaluation of tissue heterogeneity and influence on the model prediction," Journal of Biophotonics 13(2), (2020).

[135] Placzek, F., Cordero Bautista, E., Kretschmer, S., Wurster, L.M., Knorr, F., González-Cerdas, G., Erkkilä, M.T., Stein, P., Ataman, Ç., et al., "Morpho-molecular ex vivo detection and grading of non-muscle-invasive bladder cancer using forward imaging probe based multimodal optical coherence tomography and Raman spectroscopy," The Analyst 145(4), 1445–1456 (2020).

[136] Chen, H., Li, X., Broderick, N., Liu, Y., Zhou, Y., Han, J., and Xu, W., "Identification and characterization of bladder cancer by low-resolution fiber-optic Raman spectroscopy," Journal of Biophotonics 11(9), e201800016 (2018).

[137] de Jong, B.W.D., Bakker Schut, T.C., Maquelin, K., van der Kwast, T., Bangma, C.H., Kok, D.-J., and Puppels, G.J., "Discrimination between Nontumor Bladder Tissue and Tumor by Raman Spectroscopy," Analytical Chemistry 78(22), 7761–7769 (2006).

[138] Wang, L., Fan, J.-H., Guan, Z.-F., Liu, Y., Zeng, J., He, D.-L., Huang, L.-Q., Wang, X.-Y., and Gong, H.-L., "Study on bladder cancer tissues with Raman spectroscopy", Guang Pu 32(1), 123–6 (2012).

[139] Bovenkamp, D. et al., "Combination of High-Resolution Optical Coherence Tomography and Raman Spectroscopy for Improved Staging and Grading in Bladder Cancer", Appl. Sci. 8, 2371 (2018).

[140] Mukherjee, S., Wysock, J.S., Ng, C.K., Akhtar, M., Perner, S., Lee, M.-M., Rubin, M.A., Maxfield, F.R., Webb, W.W., et al., "Human bladder cancer diagnosis using multiphoton microscopy," presented at SPIE BiOS: Biomedical Optics, 12 February 2009, San Jose, CA, 716117.

[141] Cicchi, R., Crisci, A., Cosci, A., Nesi, G., Kapsokalyvas, D., Giancane, S., Carini, M., and Pavone, F.S., "Time- and Spectral-resolved two-photon imaging of healthy bladder mucosa and carcinoma in situ," Optics Express 18(4), 3840 (2010).

[142] Jain, M., Robinson, B.D., Shevchuk, M.M., Aggarwal, A., Salamoon, B., Dubin, J.M., Scherr, D.S., and Mukherjee, S., "Multiphoton Microscopy: A Potential Intraoperative Tool for the Detection of Carcinoma In Situ in Human Bladder," Archives of Pathology & Laboratory Medicine 139(6), 796–804 (2015).

[143] Katz, M.J., Huland, D.M., and Ramasamy, R., "Multiphoton microscopy: applications in Urology and Andrology" 3, (2014).

[144] Marchetti, M., Baria, E., Cicchi, R., and Pavone, F.S., "Custom Multiphoton/Raman Microscopy Setup for Imaging and Characterization of Biological Samples," Methods and Protocols 2(2), 51 (2019).

[145] Jain, M., et al., "Multiphoton Microscopy in the Evaluation of Human Bladder Biopsies," Archives of Pathology & Laboratory Medicine 136(5), 517–526 (2012).

[146] Baria, E., Barone, A., Nesi, G., Pavone, F.S., and Cicchi, R., "Imaging of human urothelial carcinoma samples using multimodal multiphoton microscopy," presented at European Conferences on Biomedical Optics, 28 July 2017, Munich, Germany, 104140Q.

[147] Frangioni, J., "In vivo near-infrared fluorescence imaging," Current Opinion in Chemical Biology 7(5), 626–634 (2003).

[148] Lim, Y.T., Kim, S., Nakayama, A., Stott, N.E., Bawendi, M.G., and Frangioni, J.V., "Selection of Quantum Dot Wavelengths for Biomedical Assays and Imaging," Molecular Imaging 2(1), 50–64 (2003).

[149] Lefort, C. "A review of biomedical multiphoton microscopy and its laser sources." Journal of physics D: Applied physics 50(42), 423001 (2017).

[150] Weber, M.J., Handbook of Laser Wavelengths. Boca Raton, FL: CRC Press, 1999. ISBN 0-8493-3508-6.

[151] Okhotnikov, O.G., Fiber Lasers. Weinheim, Germany: Wiley-VCH Verlag GmbH, 2012. ISBN 9783527411146.

[152] Denker, B., and Shklovsky, E., Handbook of solid-state lasers: materials, systems and applications. Elsevier, 2013. ISBN 978-0-85709-272-4.

[153] Poudel, C., and Kaminski, C. F., Supercontinuum radiation in fluorescence microscopy and biomedical imaging applications. Journal of the Optical Society of America B 36(2), A139–A153 (2019).

[154] Harreguy, M.B., Marfil, V., Grooms, N.W.F. et al., "Ytterbium-doped fibre femtosecond laser offers robust operation with deep and precise microsurgery of C. elegans neurons," Sci Rep 10, 4545 (2020).

[155] Zhao, Y., Nakamura, H., and Gordon, R.J., "Development of a versatile two-photon endoscope for biological imaging," Biomedical Optics Express 1(4), 1159 (2010).

[156] Rivera, D.R., Brown, C.M., Ouzounov, D.G., Pavlova, I., Kobat, D., Webb, W.W., and Xu, C., "Compact and flexible raster scanning multiphoton endoscope capable of imaging unstained tissue," Proceedings of the National Academy of Sciences 108(43), 17598–17603 (2011).

[157] Brown, C.M., Rivera, D.R., Pavlova, I., Ouzounov, D.G., Williams, W.O., Mohanan, S., Webb, W.W., and Xu, C., "In vivo imaging of unstained tissues using a compact and flexible multiphoton microendoscope," Journal of Biomedical Optics 17(4), 040505 (2012).

[158] Liang, W., Murari, K., Zhang, Y., Chen, Y., Li, M.-J., and Li, X., "Increased illumination uniformity and reduced photodamage offered by the Lissajous scanning in fiber-optic two-photon endomicroscopy," Journal of Biomedical Optics 17(2), 021108 (2012).

[159] Huland, D.M., Brown, C.M., Howard, S.S., Ouzounov, D.G., Pavlova, I., Wang, K., Rivera, D.R., Webb, W.W., and Xu, C., "In vivo imaging of unstained tissues using long gradient index lens multiphoton endoscopic systems," Biomedical Optics Express 3(5), 1077 (2012).

[160] Xi, J., Chen, Y., Zhang, Y., Murari, K., Li, M.-J., and Li, X., "Integrated multimodal endomicroscopy platform for simultaneous en face optical coherence and two-photon fluorescence imaging," Optics Letters 37(3), 362 (2012).

[161] Liang, W., Hall, G., Messerschmidt, B., Li, M.-J., and Li, X., "Nonlinear optical endomicroscopy for label-free functional histology in vivo," Light: Science & Applications 6(11), e17082–e17082 (2017).

[162] Lombardini, A., Mytskaniuk, V., Sivankutty, S., Andresen, E.R., Chen, X., Wenger, J., Fabert, M., Joly, N., Louradour, F., et al., "High-resolution multimodal flexible coherent Raman endoscope," Light: Science & Applications 7(1), 10 (2018).

[163] Dilipkumar, A., Al-Shemmary, A., Kreiß, L., Cvecek, K., Carlé, B., Knieling, F., Gonzales Menezes, J., Thoma, O., Schmidt, M., et al., "Label-Free Multiphoton Endomicroscopy for Minimally Invasive In Vivo Imaging," Advanced Science 6(8), 1801735 (2019).

[164] Ouzounov, D.G., Rivera, D.R., Williams, W.O., Stupinski, J.A., Southard, T.L., Hume, K.H., Bentley, J., Weiss, R.S., Webb, W.W., et al., "Dual modality endomicroscope with optical zoom capability," Biomedical Optics Express 4(9), 1494 (2013).

[165] Lefort, C., Hamzeh, H., Louradour, F., Pain, F., and Haidar, D.A., "Characterization, comparison, and choice of a commercial double-clad fiber for nonlinear endomicroscopy," Journal of Biomedical Optics 19(7), 076005 (2014).

[166] Ducourthial, G., Leclerc, P., Mansuryan, T., Fabert, M., Brevier, J., Habert, R., Braud, F., Batrin, R., Vever-Bizet, C., et al., "Development of a real-time flexible multiphoton microendoscope for label-free imaging in a live animal," Scientific Reports 5(1), 18303 (2015).

[167] Hamzeh, H., Lefort, C., Pain, F., and Abi Haidar, D., "Optimization and characterization of nonlinear excitation and collection through a gradient-index lens for high-resolution nonlinear endomicroscopy," Optics Letters 40(5), 808 (2015).

[168] Kim, Y., Warren, S.C., Stone, J.M., Knight, J.C., Neil, M.A.A., Paterson, C., Dunsby, C.W., and French, P.M.W., "Adaptive Multiphoton Endomicroscope Incorporating a Polarization-Maintaining Multicore Optical Fibre," IEEE Journal of Selected Topics in Quantum Electronics 22(3), 171–178 (2016).

[169] Pshenay-Severin, E., Bae, H., Reichwald, K., Matz, G., Bierlich, J., Kobelke, J., Lorenz, A., Schwuchow, A., Meyer-Zedler, T., et al., "Multimodal nonlinear endomicroscopic imaging probe using a double-core double-clad fiber and focus-combining micro-optical concept," Light: Science & Applications 10(1), 207 (2021).

[170] Sordillo, L.A., Pu, Y., Pratavieira, S., Budansky, Y., and Alfano, R.R., "Deep optical imaging of tissue using the second and third near-infrared spectral windows," Journal of Biomedical Optics 19(5), 056004 (2014).

[171] Tomilov, S., Wang, Y., Hoffmann, M., Heidrich, J., Golling, M., Keller, U., and Saraceno, C. J., "50-W average power Ho:YAG SESAM-modelocked thin-disk oscillator at 2.1 µm," Opt. Express 30, 27662-27673 (2022).

[172] Li, P., Ruehl, A., Grosse-Wortmann, U., and Hartl, I., "Sub-100 fs passively mode-locked holmium-doped fiber oscillator operating at 2.06 µm," Optics letters 39(24), 6859–6862 (2014).

[173] Rudy, C. W., Digonnet, M. J., and Byer, R. L., "Advances in 2-µm Tm-doped mode-locked fiber lasers. Optical fiber technology," 20(6), 642–649 (2014).

[174] Kamynin, V. A., Filatova, S. A., Denker, B. I., Galagan, B. I., Koltashev, V. V., Medvedkov, O. I., Sverchkov, S., and Tsvetkov, V. B., "Tm3+-doped tellurite fiber weak signal amplifier at a wavelength of 2.27 µm," Results in Physics 27, 104512 (2021).

[175] Sordillo, D. C., Sordillo, L. A., Sordillo, P. P., Shi, L., and Alfano, R. R., "Short wavelength infrared optical windows for evaluation of benign and malignant tissues," Journal of Biomedical Optics 22(4), 045002 (2017).

[176] Yamanaka, M., Teranishi, T., Kawagoe, H., and Nishizawa, N., "Optical coherence microscopy in 1700 nm spectral band for high-resolution label-free deep-tissue imaging," Scientific Reports 6(1), 31715 (2016).

[177] Sordillo, L.A., Pratavieira, S., Pu, Y., Salas-Ramirez, K., Shi, L., Zhang, L., Budansky, Y., and Alfano, R.R., "Third therapeutic spectral window for deep tissue imaging," presented at SPIE BiOS, 17 March 2014, San Francisco, California, United States, 89400V.

[178] Helmchen, F. and Denk, W., "Deep tissue two-photon microscopy," Nature Methods 2, 932-940 (2005).

[179] Xu, L., Feehan, J.S., Shen, L., Peacock, A.C., Shepherd, D.P., Richardson, D.J., and Price, J.H.V., "Yb-fiber amplifier pumped idler-resonant PPLN optical parametric oscillator producing 90 femtosecond pulses with high beam quality," Applied Physics B 117(4), 987–993 (2014).

[180] Krauth, J., Steinmann, A., Hegenbarth, R., Conforti, M., and Giessen, H., "Broadly tunable femtosecond near- and mid-IR source by direct pumping of an OPA with a 417 MHz Yb:KGW oscillator," Optics Express 21(9), 11516 (2013).

[181] Fan, J., Gu, C., Zhao, J., Liao, R., Chu, Y., Chai, L., Wang, C., and Hu, M., "Dielectric-mirror-less femtosecond optical parametric oscillator with ultrabroad-band tunability," Optics Letters 43(10), 2316 (2018).

[182] Kiani, L., Lu, T., and Sharping, J.E., "Comparison of amplitude noise of a fiber-optical parametric oscillator and a supercontinuum source," Journal of the Optical Society of America B 31(8), 1986 (2014).

[183] O'Connor, M.V., Watson, M.A., Shepherd, D.P., Hanna, D.C., Price, J.H.V., Malinowski, A., Nilsson, J., Broderick, N.G.R., Richardson, D.J., et al., "Synchronously pumped optical parametric oscillator driven by a femtosecond mode-locked fiber laser," Optics Letters 27(12), 1052 (2002).

[184] Mörz, F., Steinle, T., Steinmann, A., and Giessen, H., "Multi-Watt femtosecond optical parametric master oscillator power amplifier at 43 MHz," Optics Express 23(18), 23960 (2015).

[185] Steinle, T., Mörz, F., Steinmann, A., and Giessen, H., "Ultra-stable high average power femtosecond laser system tunable from 133 to 20 µm," Optics Letters 41(21), 4863 (2016).

[186] Tzeng, Y.-W., Huang, C.-H., Lin, Y.-Y., Liu, J.-M., Chui, H.-C., Liu, H.-L., Stone, J.M., Knight, J.C., and Chu, S.-W., "High repetition rate optical parametric amplification based on a single Yb:fiber laser," in Conference on Lasers and Electro-Optics/International Quantum Electronics Conference, CWJ7 (2009).

[187] Rigaud, P., Van de Walle, A., Hanna, M., Forget, N., Guichard, F., Zaouter, Y., Guesmi, K., Druon, F., and Georges, P., "Supercontinuum-seeded few-cycle mid-infrared OPCPA system," Optics Express 24(23), 26494 (2016).

[188] Kanai, T., Lee, Y., Seo, M., and Kim, D.E., "Supercontinuum-seeded, carrier-envelope phase-stable, 45-W, 38-µm, 6-cycle, KTA optical parametric amplifier driven by a 14-ps Yb:YAG thin-disk amplifier for nonperturbative spectroscopy in solids," Journal of the Optical Society of America B 36(9), 2407 (2019).

[189] Becheker, R., Tang, M., Hanzard, P.-H., Tyazhev, A., Mussot, A., Kudlinski, A., Kellou, A., Oudar, J.-L., Godin, T., et al., "High-energy dissipative soliton-driven fiber optical parametric oscillator emitting at 1.7 µ m," Laser Physics Letters 15(11), 115103 (2018).

[190] Hanna, M., Druon, F., and Georges, P., "Fiber optical parametric chirped-pulse amplification in the femtosecond regime," Opt. Express, 14(7), 2783 (2006).

[191] Cristofori, V., Lali-Dastjerdi, Z., Rishøj, L.S., Galili, M., Peucheret, C., and Rottwitt, K., "Dynamic characterization and amplification of sub-picosecond pulses in fiber optical parametric chirped pulse amplifiers," Opt. Express, 21(22), 26044 (2013).

[192] Qin, Y., Batjargal, O., Cromey, B., and Kieu, K., "High-power 1700 nm femtosecond laser based on optical parametric chirped-pulse amplification," Conference on Lasers and Electro-Optics, STh1P.5 (2020).

[193] Qin, Y., Batjargal, O., Cromey, B., and Kieu, K., "All-fiber high-power 1700 nm femtosecond laser based on optical parametric chirped-pulse amplification," Opt. Express, 28(2), 2317 (2020).

[194] Roy, R., Schulz, P.A., and Walther, A., "Acousto-optic modulator as an electronically selectable unidirectional device in a ring laser," Opt. Lett., 12(9), 672 (1987).

[195] Yang, K., Zhao, P., Luo, J., Huang, K., Hao, Q., Zeng, H., "Comparison on different repetition rate locking methods in Er-doped fiber laser", Laser Phys., 28, 055108 (2018).

[196] Korobko, D.A., Stoliarov, Ribenek, V.A., D.A., Itrin, P.A., Odnoblyudov, M.A., Petrov, A.B., and Gumenyuk, R.V., "Harmonic mode-locking fiber ring laser with a pulse repetition rate up to 12 GHz," Opt. Laser Technol., 133, 106526 (2021).

[197] Stoliarov, D.A., Itrin, P.A., Ribenek, V.A., Korobko, D.A., Fotiadi, A.A., "Linear cavity fiber laser harmonically mode-locked with SESAM", Laser Phys. Lett., 17, 105102 (2020).

[198] Ribenek, V.A., Stoliarov, D.A., Korobko, D.A., and Fotiadi, A.A., "Mitigation of the supermode noise in a harmonically mode-locked ring fiber laser using optical injection," Opt. Lett., 46, 5747-5750 (2021).

[199] Khegai, A., Melkumov, M., Riumkin, K., Khopin, V., Firstov, S., and Dianov, E., "NALM-based bismuth-doped fiber laser at 1.7 μm," Opt. Lett., 43(5), 1127 (2018).

[200] Fujimoto, Y., and Nakatsuka, M., "Infrared Luminescence from Bismuth-Doped Silica Glass," Jpn. J. Appl. Phys., 40(Part 2, No. 3B), L279–L281 (2001).

[201] Noronen, T., Melkumov, M., Stolyarov, D., Khopin, V.F., Dianov, E., and Okhotnikov, O.G., "All-bismuth fiber system for femtosecond pulse generation, compression, and energy scaling," Optics Letters 40(10), 2217 (2015).

[202] Firstov, S.V., Alyshev, S.V., Riumkin, K.E., Khegai, A.M., Kharakhordin, A.V., Melkumov, M.A., and Dianov, E.M., "Laser-Active Fibers Doped With Bismuth for a Wavelength Region of 1.6–1.8 μm," IEEE Journal of Selected Topics in Quantum Electronics 24(5), 1–15 (2018).

[203] Noronen, T., Firstov, S., Dianov, E., and Okhotnikov, O.G., "1700 nm dispersion managed mode-locked bismuth fiber laser," Scientific Reports 6(1), 24876 (2016).

[204] Emami, S.D., Dashtabi, M.M., Lee, H.J., Arabanian, A.S., and Rashid, H.A.A., "1700 nm and 1800 nm band tunable thulium doped mode-locked fiber lasers," Scientific Reports 7(1), 12747 (2017).

[205] Xinyang Liu, Jayanta K. Sahu, and Regina Gumenyuk, "Tunable dissipative soliton Tm-doped fiber laser operating from 1700 nm to 1900 nm," Opt. Lett. 48, 612-615 (2023).

[206] Stolen, R., Lin, C., "Self-phase-modulation in silica optical fibers", Phys. Rev. A 17 (4), 1448 (1978)

[207] Islam, M.N., Simpson, J.R., Shang, H.T., Mollenauer, L.F., and Stolen, R.H., "Cross-phase modulation in optical fibers," Optics Letters 12(8), 625 (1987).

[208] Stolen, R., "Phase-matched-stimulated four-photon mixing in silica-fiber waveguides," IEEE Journal of Quantum Electronics 11(3), 100–103 (1975).

[209] Eckhardt, G., Bortfeld, D.P., and Geller, M., "Stimulated emission of Stokes and anti-Stokes Raman lines from diamond, calcite, and α-sulfur single crystals," Appl. Phys. Lett. 3(8), 137-138 (1963).

[210] Smith, R.G., "Optical Power Handling Capacity of Low Loss Optical Fibers as Determined by Stimulated Raman and Brillouin Scattering," Applied Optics 11(11), 2489 (1972).

[211] Chiao, R.Y., Townes, C.H., and Stoicheff, B.P., "Stimulated Brillouin Scattering and Coherent Generation of Intense Hypersonic Waves," Physical Review Letters 12(21), 592–595 (1964).

[212] Ippen, E.P., "Low-power quasi-cw Raman oscillator," Appl. Phys. Lett. 16(8), 303-305 (1970).

[213] Agrawal, G.P., "Nonlinear fiber optics: its history and recent progress " J. Opt. Soc. Am. B 28(12), A1 (2011).

[214] He, X., Lin, Q., Guo, H., Sun, J., Bai, J., Hou, L., and Wang, K., "Robust 1.7- μ m, all-polarization-maintaining femtosecond fiber laser source based on standard telecom fibers," Applied Physics Express 12(7), 072007 (2019).

[215] Fang, X., Wang, Z., and Zhan, L., "Efficient generation of all-fiber femtosecond pulses at 1.7 μ m via soliton self-frequency shift," Optical Engineering 56(4), 046107 (2017).

[216] Chung, H.Y., Liu, W., Cao, Q., Kärtner, F.X., and Chang, G., "Er-fiber laser enabled, energy scalable femtosecond source tunable from 1.3 to 1.7 μm," Opt. Express 25, 15760-15771 (2017).

[217] Cadroas, P., Abdeladim, L., Kotov, L., Likhachev, M., Lipatov, D., Gaponov, D., Hideur, A., Tang, M., Livet, J., et al., "All-fiber femtosecond laser providing 9 nJ, 50 MHz pulses at 1650 nm for three-photon microscopy," J. Opt. 19(6), 065506 (2017).

[218] Stoliarov, D., Koviarov, A., Korobko, D., Galiakhmetova, D., Rafailov, E., "Fibre laser system with wavelength tuning in extended telecom range," Opt. Fiber Technol. 72, 2022.

[219] Wang, K., Horton, N.G., Charan, K., and Xu, C., "Advanced fiber soliton sources for nonlinear deep tissue imaging in biophotonics," IEEE J. Sel. Top. Quantum Electron. 20, 6800311 (2014).

[220] Zanoni, M., Piccinini, F., Arienti, C., Zamagni, A., Santi, S., Polico, R., Bevilacqua, A., and Tesei, A., "3D tumor spheroid models for in vitro therapeutic screening: a systematic approach to enhance the biological relevance of data obtained," Scientific Reports 6(1), 19103 (2016).

[221] Zanoni, M., Cortesi, M., Zamagni, A., Arienti, C., Pignatta, S., and Tesei, A., "Modeling neoplastic disease with spheroids and organoids," Journal of Hematology & Oncology 13(1), 97 (2020).

[222] Kastner, C., Hendricks, A., Deinlein, H., Hankir, M., Germer, C.-T., Schmidt, S., and Wiegering, A., "Organoid Models for Cancer Research-From Bed to Bench Side and Back," Cancers 13(19), 4812 (2021).

[223] Sachs, N., de Ligt, J., Kopper, O., Gogola, E., Bounova, G., Weeber, F., Balgobind, A.V., Wind, K., Gracanin, A., et al., "A Living Biobank of Breast Cancer Organoids Captures Disease Heterogeneity," Cell 172(1–2), 373-386.e10 (2018).

[224] Atat, O.E., Farzaneh, Z., Pourhamzeh, M., Taki, F., Abi-Habib, R., Vosough, M., and El-Sibai, M., "3D modeling in cancer studies," Human Cell 35(1), 23–36 (2022).

[225] Palmer, S., Litvinova, K., Dunaev, A., Fleming, S., McGloin, D., and Nabi, G., "Changes in autofluorescence based organoid model of muscle invasive urinary bladder cancer," Biomedical Optics Express 7(4), 1193–1200 (2016).

[226] Banerjee, S., and Southgate, J., "Bladder organoids: a step towards personalised cancer therapy?," Translational Andrology and Urology 8(Suppl 3), S300–S302 (2019).

[227] Seidlitz, T., and Stange, D.E., "Gastrointestinal cancer organoids-applications in basic and translational cancer research," Experimental & Molecular Medicine 53(10), 1459–1470 (2021).

[228] Zhang, R., Guo, T., Ji, L., Yin, Y., Feng, S., Lu, W., Zhang, F., Zhu, M., Liu, S., et al., "Development and Application of Patient-Derived Cancer Organoidsin Clinical Management of Gastrointestinal Cancer: A State-of-the-Art Review," Frontiers in Oncology 11, 716339 (2021).

[229] Yoshida, T., Sopko, N.A., Kates, M., Liu, X., Joice, G., Mcconkey, D.J., and Bivalacqua, T.J., "Impact of spheroid culture on molecular and functional characteristics of bladder cancer cell lines," Oncology Letters 18(5), 4923–4929 (2019).

[230] Kim, H., Han, Y., Suhito, I.R., Choi, Y., Kwon, M., Son, H., Kim, H.-R., and Kim, T.-H., "Raman Spectroscopy-Based 3D Analysis of Odontogenic Differentiation of Human Dental Pulp Stem Cell Spheroids," Analytical Chemistry 93(29), 9995–10004 (2021).

[231] Gil, D.A., Deming, D., and Skala, M.C., "Patient-derived cancer organoid tracking with wide-field one-photon redox imaging to assess treatment response," Journal of Biomedical Optics 26(3), (2021).

[232] Pasquale, V., Ducci, G., Campioni, G., Ventrici, A., Assalini, C., Busti, S., Vanoni, M., Vago, R., and Sacco, E., "Profiling and Targeting of Energy and Redox Metabolism in Grade 2 Bladder Cancer Cells with Different Invasiveness Properties," Cells 9(12), E2669 (2020).

[233] Walsh, A.J., Cook, R.S., and Skala, M.C., "Functional Optical Imaging of Primary Human Tumor Organoids: Development of a Personalized Drug Screen," Journal of Nuclear Medicine 58(9), 1367–1372 (2017).

[234] Hu, L.-F., Yang, X., Lan, H.-R., Fang, X.-L., Chen, X.-Y., and Jin, K.-T., "Preclinical tumor organoid models in personalized cancer therapy: Not everyone fits the mold," Experimental Cell Research 408(2), 112858 (2021).

**Annex**

**Table A1.** List of studies reporting the detection of gastrointestinal tumours by fluorescence spectroscopy.

| Paper | Year | Type | Patients* (N-T; T) | Sites* (N-T; T) | $\lambda_{exc}$ (nm) | Sens. (%) | Spec. (%) |
|---|---|---|---|---|---|---|---|
| R. M. Cothren et al.[62] | 1990 | in vivo | 20 | 67 (36; 31) | | 100 | 97 |
| C. R. Kapadia et al.[59] | 1990 | ex-vivo | | 70 (35; 35) | 325 | 100 | 100 |
| R. Marchesini et al.[60] | 1992 | ex-vivo | 45 (9; 36) | 78 (42; 36) | 410 | 80.6 | 90.5 |
| B. W. Chwirot et al.[61] | 1997 | ex-vivo | 21 | 72 (50; 23) | 325 | 96 | 52 |
| M. Kobayashi et al.[68] | 2001 | in vivo | 52 | 54 (21; 33) | 437 | 94 | 86 |
| B. Mayinger et al.[69] | 2001 | in vivo | 13 | 129 (57; 72) | 375-478 | 97 | 95 |
| S. D. Xiao et al.[70] | 2002 | in vivo | 38 (21; 17) | | 442 | 83 | 91 |
| B. Mayinger et al.[71] | 2004 | in vivo | 31 | | 375-478 | 69 | 87 |
| S. D. Kamath et al.[72] | 2008 | ex-vivo | | 23 (13, 10) | 325 | 93.5 | 100 |
| M. S. Bergholt et al.[73] | 2011 | in vivo | 81 | 176 | 785 | 98.6 | 84.7 |
| D. F. Boerwinkel et al.[74] | 2015 | in vivo | 47 (12; 35) | 151 (108; 43) | 405 | 81 | 58 |
| L. Ehlen et al.[75] | 2019 | ex-vivo | 10 | 95 (45; 50) | 473 | 87 | 78 |
| **MEAN ± SD** | | | | | | **90 ± 10** | **85 ± 15** |

***** Number of patients and tissue areas/biopsies effectively included in each study, i.e. non-counting the ones excluded from analysis due to artefacts or other reasons. In brackets, the number of non-tumour (N-T) and tumour (T) sites.

**Table A2.** List of studies reporting the detection of gastrointestinal tumours by reflectance spectroscopy or imaging.

| Paper | Year | Type | Patients* | Sites* (N-T; T) | Detection (nm) | Sens. (%) | Spec. (%) |
|---|---|---|---|---|---|---|---|
| Z. Ge et al.[63] | 1998 | in vivo | | 160 (107; 53) | 350-800 | 85** | 85** |
| A. Dhar et al.[76] | 2006 | in vivo | 45 | 138 | 300-800 | 80 | 86 |
| H. Akbari et al.[77] | 2011 | ex-vivo | 10 | 101 | 1000-2500 | 91 | 93 |
| S. Kiyotoki et al.[78] | 2013 | ex-vivo | 14 | 320 (160; 160) | 400-800 | 76.2 | 78.8 |
| D. J. Evers et al.[79] | 2013 | ex-vivo | 24 | 828 (393; 435) | 500-1600 | 94 | 94 |
| R. Kumashiro et al.[80] | 2016 | in vivo | 24 | 135 (95; 40) | 450-600 | 72.5 | 82.1 |
| Z. Han et al.[81] | 2016 | in vivo | 12 | 21 | 405-665 | 97 | 91 |
| E. Tanis et al.[82] | 2016 | in vivo | 17 | 484 | 400-1600 | 95 | 92 |
| A. Keller et al.[83] | 2018 | ex-vivo | 32 | 254 (123; 131) | 344-1044 | 98.4 | 99.2 |
| L. Ehlen et al.[75] | 2019 | ex-vivo | 10 | 95 (45; 50) | 901-1301 | 93 | 68 |
| E. J. M. Baltussen et al.[84] | 2019 | in vivo | 32 | 270 | 400-1700 | 90 | 94 |
| M. S. Nogueira et al.[85] | 2021 | ex-vivo | 47 | | 350-1919 | 96.1 | 95.7 |
| **MEAN ± SD** | | | | | | **89 ± 9** | **88 ± 9** |

***** Number of patients and tissue areas/biopsies effectively included in each study, i.e. non-counting the ones excluded from analysis due to artefacts or other reasons. In brackets, the number of non-tumour (N-T) and tumour (T) sites.
** Values corresponding to the mean predictive accuracy.

**Table A3.** List of studies reporting the detection of gastrointestinal tumours by Raman spectroscopy.

| Paper | Year | Type | Patients* (N-T; T) | Sites* (N-T; T) | Spectra (N-T; T) | $\lambda_{exc}$ (nm) | Sens. (%) | Spec. (%) |
|---|---|---|---|---|---|---|---|---|
| N. Stone et al.[65] | 2002 | ex-vivo | 44 | 89 | 617 (455; 162) | 830 | 94 | 93 |
| C. Kendall et al.[66] | 2003 | ex-vivo | 44 | 87 (53; 34) | 1125 | 830 | 94 | 93 |
| S. K. Teh et al.[67] | 2008 | ex-vivo | 53 | 73 (55; 18) | 222 (143; 79) | 785 | 90.2 | 95.7 |
| Z. Huang et al.[86] | 2010 | in vivo | 67 | 238 (121; 117) | 1063 | 785 | 94.0 | 93.4 |
| S. K. Teh et al.[87] | 2010 | ex-vivo | 62 | 100 (70; 30) | | 785 | 80 | 91 |
| M. S. Bergholt et al.[88] | 2011 | in vivo | 67 (63; 61) | 238 (121; 117) | 1063 (934; 129) | 785 | 94.6 | 94.6 |
| M. S. Bergholt et al.[73] | 2011 | in vivo | 81 | 176 | 1238 (1098; 140) | 785 | 92.9 | 89.3 |
| T. Kawabata et al.[89] | 2011 | ex-vivo | 10 | | 213 (132; 81) | 1040 | 73 | 73 |
| S. Duraipandian et al.[90] | 2012 | in vivo | 305 | | 2748 (2465; 283) | 785 | 80.5 | 86.2 |
| M. S. Bergholt et al.[91] | 2013 | in vivo | 83 | | 1277 (1013; 264) | 785 | 84.9 | 95.6 |
| S. Jin et al.[92] | 2014 | ex-vivo | 105 (72; 33) | | | NIR | 100 | 97.4 |
| J. Wang et al.[93] | 2016 | in vivo | 191 (178; 13) | 441 (407; 34) | 5792 (5315; 477) | 785 | 82.4 | 94.3 |
| D. Petersen et al.[94] | 2017 | ex-vivo | 69 (56, 13) | 123 (101, 22) | 269 (204, 65) | 785 | 79 | 83 |
| **MEAN ± SD** | | | | | | | **88 ± 8** | **91 ± 7** |

***** Number of patients and tissue areas/biopsies effectively included in each study, i.e. non-counting the ones excluded from analysis due to artefacts or other reasons. In brackets, the number of non-tumour (N-T) and tumour (T) sites.

**Table A4.** List of studies reporting the detection of gastrointestinal cancer by nonlinear techniques.

| Author | Tissue | Signal collected | Type | λexc (nm) | Year |
|---|---|---|---|---|---|
| W. Zheng **et al.**[99] | Oral cheek pouch | TPEF/SHG | in-vivo | 745 | 2011 |
| **R. Orzekowsky-Schroeder et al.**[100] | Small intestine | TPEF** | in-vivo | 730-910 | 2011 |
| R. Cicchi et al.[101] | Colon mucosa | TPEF | ex-vivo | 740 | 2013 |
| T. Makino et al.[102] | Oesophagus, stomach, duodenum, ileum, and colon | SHG/TPEF | ex-vivo | 780 | 2013 |
| J. Chen et al.[103] | Oesophagus, gastroesophageal junction (GEJ), and gastric cardia * | TPEF**/SHG | ex-vivo | 735/800 | 2014 |
| S. G. Stanciu **et al.**[104] | Liver | TPEF/SHG | ex-vivo | 900 | 2014 |
| L. Li et al.[105] | Colorectal | TPEF/SHG | ex-vivo | 810 | 2014 |
| A. Schueth et al.[106] | Bladder | TPEF/SHG | ex-vivo | 800 | 2014 |
| J. Yan et al.[107] | Rectal | TPEF/SHG | ex-vivo | 800 | 2014 |
| A. Klinger et al.[51] | Murine intestinal mucosa | TPEF** | in-vivo | 730/800 vs 800 (10fs) | 2015 |
| Y. Zhou et al.[108] | Gastric muscularis propria * | TPEF/SHG | ex-vivo | 810 | 2016 |
| M. Skala et al.[109] | Hamster cheek pouch | SHG/ TPEF | ex-vivo | 780 | 2017 |
| T. Matsui et al.[110] | Colorectal * | TPEF**/SHG | ex-vivo | 730/ 820/ 900 | 2017 |
| B. Sarri et al.[111] | Colon pancreas* | SRS/SHG/CARS/ TPEF | ex-vivo | 1030+790-800 | 2019 |
| L. Li et al.[112] | Gastric | TPEF/SHG | ex-vivo | 810 | 2019 |
| W.-C. Chen **et al.**[43] | Oesophagus * | TPEF/SHG | ex-vivo | 810 | 2020 |
| B. Shen **et al.**[113] | Pancreas and liver | THG/FLIM/3PEF/ TPEF/SHG | in-vivo | 1140 | 2020 |
| H. Zhang **et al.**[114] | Laryngeal squamous | 3PFE/SHG/ THG | ex-vivo | 1050 (40fs) | 2021 |

**Table A5.** List of studies reporting the detection of bladder tumours by fluorescence spectroscopy.

| Paper | Year | Type | Patients* | Sites* (N-T; T) | $\lambda_{exc}$ (nm) | Sens. (%) | Spec. (%) |
|---|---|---|---|---|---|---|---|
| M. A. D'Hallewin et al.[115] | 1994 | in vivo | >10 | | 365 | | |
| F. Koenig et al.[116] | 1996 | in vivo | 53 | 114 (29; 85) | 337 | 97 | 98 |
| M. Anidjar et al.[120] | 1996 | ex-vivo | | 21 (9; 12) | 308 | 100 | 100 |
| D. Zaak et al.[117] | 2002 | in vivo | 43 | 114 (21; 93) | 308 | 95 | 77 |
| W. Zheng et al.[121] | 2003 | ex-vivo | 25 | 52 (14; 38) | 280<br>330 | 97<br>95 | 93<br>92 |
| O. Aboumarzouk et al.[118] | 2015 | in vivo | 21 | 63 (37; 30) | 405 | | |
| M. C. Kriegmair et al.[119] | 2018 | in vivo | 25 | 56 (26; 30) | 440 | 96.7 | 53.8 |
| E. Baria et al.[60] | 2019 | ex-vivo | 32 | 50 (20; 30) | 378<br>445 | 100<br>95 | 100<br>100 |
| S. Morselli et al.[61] | 2021 | ex-vivo | 114 | 169 (40; 129) | 378<br>445 | 79<br>70 | 80<br>89 |
| **MEAN ± SD** | | | | | | **92 ± 10** | **88 ± 15** |

***** Number of patients and tissue areas/biopsies effectively included in each study, i.e. non-counting the ones excluded from analysis due to artefacts or other reasons. In brackets, the number of non-tumour (N-T) and tumour (T) sites.

**Table A6.** List of studies reporting the detection of bladder tumours by reflectance spectroscopy or imaging.

| Paper | Year | Type | Patients* (N-T; T) | Sites* (N-T; T) | Detection (nm) | Sens. (%) | Spec. (%) |
|---|---|---|---|---|---|---|---|
| J. R. Mourant et al.[122] | 1995 | in vivo | 10 | 50 (30; 20) | 250-800 | 100 | 97 |
| F. Koenig et al.[123] | 1998 | in vivo | 14 | 26 (17; 9) | 450-700 | 91 | 60 |
| H. W. Herr et al.[126] | 2008 | in vivo | 427 | | 415 ± 30<br>540 ± 30 | 100 | 82 |
| K. Tatsugami[127] | 2010 | in vivo | 104 | 313 | 415 ± 30<br>540 ± 30 | 92.7 | 70.9 |
| G. Chen et al.[128] | 2013 | in vivo | 143 | (NA; 285) | 415 ± 30<br>540 ± 30 | 79 | 79 |
| Z. Ye et al.[129] | 2015 | in vivo | 103 (16; 87) | 300 | 415 ± 30<br>540 ± 30 | 98.8 | 60.9 |
| J. Slaton et al.[124] | 2016 | in vivo** | 6 (2; 4) | 108 (27; 81) | 520-920 | | |
| E. Baria et al.[60] | 2019 | ex-vivo | 32 | 50 (20; 30) | 440-710 | 90 | 83 |
| S. Morselli et al.[61] | 2021 | ex-vivo | 114 | 169 (40; 129) | 440-710 | 66 | 65 |
| **MEAN ± SD** | | | | | | **90 ± 12** | **75 ± 13** |

***** Number of patients and tissue areas/biopsies effectively included in each study, i.e. non-counting the ones excluded from analysis due to artefacts or other reasons. In brackets, the number of non-tumour (N-T) and tumour (T) sites.
****** Study conducted on animal model.

**Table A7.** List of studies reporting the detection of bladder tumours by Raman spectroscopy.

| Paper | Year | Type | Patients* | Sites* (N-T; T) | Spectra (N-T; T) | $\lambda_{exc}$ (nm) | Sens. (%) | Spec. (%) |
|---|---|---|---|---|---|---|---|---|
| N. Stone et al.[65] | 2002 | ex-vivo | 12 | 12 | 196 (15; 181) | 830 | 99 | 93 |
| P. Crow et al.[130] | 2004 | ex-vivo | 72 | 75 | 1525 | 830 | 97 | 95 |
| P. Crow et al.[131] | 2005 | ex-vivo | | 29 | 220 | 785 | 79 | 89 |
| B.W.D. de Jong et al.[137] | 2006 | ex-vivo | 15 | 90 (37; 53) | | 845 | 94 | 92 |
| R. O. P. Draga et al.[132] | 2010 | in vivo | 32 | | 63 (28; 35) | 785 | 85 | 79 |
| I. Barman et al.[133] | 2012 | ex-vivo | 14 | 28 (14; 14) | 140 (70; 70) | 785 | 85.7 | 100 |
| L. Wang et al.[138] | 2012 | ex-vivo | | | | 632.8 | 87.7 | 87.5 |
| H. Chen et al.[136] | 2018 | ex-vivo | 10 | 32 | 262 (78; 184) | 785 | 95.1 | 88.5 |
| E. Baria et al.[60] | 2019 | ex-vivo | 32 | 50 (20; 30) | 50 (20; 30) | 785 | 95 | 87 |
| E. Cordero et al.[134] | 2019 | ex-vivo | 21 | 48 | | 785 | 92 | 93 |
| F. Placzek et al.[135] | 2020 | ex-vivo | 44 | 116 (66; 50) | ~100000 | 785 | 95 | 88 |
| S. Morselli et al.[61] | 2021 | ex-vivo | 114 | 169 (40; 129) | 169 (40; 129) | 785 | 77 | 72 |
| **MEAN ± SD** | | | | | | | **90 ± 7** | **89 ± 7** |

***** Number of patients and tissue areas/biopsies effectively included in each study, i.e. non-counting the ones excluded from analysis due to artefacts or other reasons. In brackets, the number of non-tumour (N-T) and tumour (T) sites.

**Table A8.** List of studies reporting the discrimination between LG and HG bladder tumours by Raman spectroscopy.

| Paper | Year | Type | $\lambda_{exc}$ (nm) | Sens. (%) | Spec. (%) |
|---|---|---|---|---|---|
| P. Crow et al.[130] | 2004 | ex-vivo | 830 | 98* | 93* |
| D. Bovenkamp et al.[139] | 2018 | ex-vivo | 785 | 99 | 87 |
| H. Chen et al.[136] | 2018 | ex-vivo | 785 | 97.5* | 96.4* |
| E. Baria et al.[60] | 2019 | ex-vivo | 785 | 90 | 90 |
| E. Cordero et al.[134] | 2019 | ex-vivo | 785 | 85 | 83 |
| F. Placzek et al.[135] | 2020 | ex-vivo | 785 | 81 | 68 |
| S. Morselli et al.[61] | 2021 | ex-vivo | 785 | 73 | 65 |
| **MEAN ± SD** | | | | **89 ± 10** | **83 ± 12** |

*These values represent sensitivity and specificity in discriminating HG spectra from both non-tumour and LG spectra.

**Table A9.** List of studies reporting the detection of bladder tumours by non-linear techniques.

| Paper | Tissue | Technique | Year | $\lambda_{exc}$ (nm) | Type |
|---|---|---|---|---|---|
| S. Mukherjee et al.[140] | Bladder | SHG/TPEF | 2009 | 785 | ex-vivo |
| R. Cicchi et al.[141] | Bladder | SHG/TPEF/FLIM | 2010 | 790 | ex-vivo |
| M. Jain et al.[142] | Bladder | SHG/TPEF | 2012 | 785 | ex-vivo |
| M. J. Katz et al.[143] | Bladder- prostate | SHG/TPEF | 2014 | 785 | ex-vivo |
| M. Jain et al.[145] | Bladder | SHG/TPEF | 2015 | 785 | ex-vivo |
| M. Marchetti et al.[144] | Bladder | ALL | 2019 | 1040+785 | ex-vivo |

**Table A10.** List of studies reporting multimodal techniques using an endoscope.

| Author | Tissue | Non-linear effect reported | Excitation wavelength [nm] | Year |
|---|---|---|---|---|
| Y. Zhao et al.[155] | Human Trabecular (stained) | TPEF | 800 | 2010 |
| D. R. Rivera et al.[156] | Mouse tail tendon<br>Mouse colon<br>Mouse lung | TPEF/SHG | 800 | 2011 |
| C. M. Brown et al.[157] | Rat kidney (ex-vivo)<br>Rat colon (in-vivo) | TPEF/SHG | 800 | 2012 |
| D. M. Huland et al.[158] | Rat kidney renal cortex<br>Rat inner colon wall<br>Rat liver | TPEF/SHG | 800 | 2012 |
| J. Xi et al.[159] | A431 cancer cells (stained) | TPEF/OCT | 1550 | 2012 |
| W. Liang et al.[160] | Mouse liver (ex-vivo)<br>Mouse small intestine (in-vivo) | TPEF/SHG | 810 | 2017 |
| A. Lombardini et al.[162] | Human colon fatty tissues | SHG/CARS | 800/1040 | 2018 |
| A. Dilipkumar et al.[163] | Murine colon mucosa in vivo | TPEF/SHG | 780 | 2019 |

**Table A11.** List of studies reporting improvements in the microendoscope.

| Author | Non-linear effect reported | Excitation wavelength [nm] | Year | Improvement provided |
|---|---|---|---|---|
| W. Liang et al.[158] | TPEF | 810 | 2012 | Increased illumination uniformity and reduced photodamage |
| D. G. Ouzounov et al.[164] | TPEF | 800 | 2013 | Add optical zoom capability |
| C. Lefort et al.[165] | TPEF | 800 | 2014 | Improving and characterising of a commercial double-clad fiber |
| G. Ducourthial et al.[166] | TPEF/SHG | 810 | 2015 | Improving acquisition time |
| H. Hamzeh et al.[167] | TPEF | 750-810 | 2015 | Optimization and characterisation of GRIN lens |
| Y. Kim et al.[168] | TPEF | | 2016 | Incorporating a Polarization Maintaining |
| E. Pshenay-Severin et al.[169] | CARS, TPEF, SHG | 795/1030 | 2021 | Laser transmission and signal collection for CARS, SHG, and TPEF |